© 2023. Published by The Company of Biologists Ltd | Journal of Cell Science (2023) 136, jcs260060. doi:10.1242/jcs.260060

RESEARCH ARTICLE

Functional crosstalk between the TIM22 complex and YME1 machinery maintains mitochondrial proteostasis and integrity

Abhishek Kumar, Tejashree Pradip Waingankar and Patrick D'Silva*

ABSTRACT

TIM22 pathway cargos are essential for sustaining mitochondrial homeostasis as an excess of these proteins leads to proteostatic stress and cell death. Yme1 is an inner membrane metalloprotease that regulates protein quality control with chaperone-like and proteolytic activities. Although the mitochondrial translocase and protease machinery are critical for organelle health, their functional association remains unexplored. The present study unravels a novel genetic connection between the TIM22 complex and YME1 machinery in *Saccharomyces cerevisiae* that is required for maintaining mitochondrial health. Our genetic analyses indicate that impairment in the TIM22 complex rescues the respiratory growth defects of cells without Yme1. Furthermore, Yme1 is essential for the stability of the TIM22 complex and regulates the proteostasis of TIM22 pathway substrates. Moreover, impairment in the TIM22 complex suppressed the mitochondrial structural and functional defects of Yme1-devoid cells. In summary, excessive levels of TIM22 pathway substrates could be one of the reasons for respiratory growth defects of cells lacking Yme1, and compromising the TIM22 complex can compensate for the imbalance in mitochondrial proteostasis caused by the loss of Yme1.

KEY WORDS: Mitochondrial protein translocation, Mitochondrial proteostasis, Mitochondrial quality control, Mitochondrial DNA maintenance, TIM22 complex, YME1 machinery

INTRODUCTION

Mitochondria are often referred to as the powerhouse of the cell due to their ability to generate ATP. However, apart from energy conversion, this organelle is also involved in diverse cellular processes, including iron–sulfur cluster production, biosynthesis of several metabolites and apoptosis (Lill and Mühlenhoff, 2005; Nunnari and Suomalainen, 2012; Kang et al., 2018). Therefore, proper mitochondrial function is paramount for cell survival, and any impairment in mitochondrial health could be detrimental to cells. Mitochondria encompass a wide variety of proteins to execute these essential cellular functions, most of which are encoded by the nuclear genome, translated in the cytosol, and subsequently translocated into different mitochondrial subcompartments with the help of specialized protein-conducting machinery known as translocases (Baker et al., 2007; Neupert and Herrmann, 2007; Endo and Yamano, 2009; Wiedemann and Pfanner, 2017). The translocase of the outer membrane (TOM) complex functions as a general entry gate for most incoming mitochondrial proteins (Dukanovic and Rapaport, 2011; Araiso et al., 2019). On the contrary, the inner membrane (IM) contains two translocases: the TIM23 complex (presequence translocase) and the TIM22 complex (carrier translocase) (Chacinska et al., 2009; Schmidt et al., 2010; Dudek et al., 2013). The TIM23 complex mediates the sorting of proteins with presequences into the IM and the matrix, whereas the TIM22 complex integrates polytopic membrane proteins into the IM (Sirrenberg et al., 1996; Rehling et al., 2004; van der Laan et al., 2010; Schendzielorz et al., 2018; Kumar et al., 2022).

The TIM22 complex is evolutionarily conserved across the eukaryotic system, but its composition differs from yeast to humans. In yeast, the TIM22 complex is a 300-kDa insertase machinery consisting of the membrane subunits Tim22, Tim54, Sdh3 and Tim18, and small Tim proteins Tim9, Tim10 and Tim12 (Jarosch et al., 1996, 1997; Kerscher et al., 1997, 2000; Adam et al., 1999; Koehler et al., 2000; Kovermann et al., 2002; Gebert et al., 2011; Stojanovski et al., 2012). Tim22 forms the central core channel, and its conserved regions play a critical role in recruiting the partner subunits to assemble the functional translocase (Rehling et al., 2003; Kumar et al., 2020; Zhang et al., 2021). On the other hand, Tim18 and Sdh3 provide stability to the TIM22 complex, whereas Tim54 acts as an adaptor protein for docking of small Tim chaperones (Kerscher et al., 2000; Koehler et al., 2000; Wagner et al., 2008; Gebert et al., 2011). The small Tim proteins assist in transferring hydrophobic client proteins from the TOM complex to the TIM22 complex (Wagner et al., 2008; Weinhäupl et al., 2021). The TIM22 pathway consists of an additional hexameric complex formed by another class of small Tim proteins, Tim8 and Tim13, required for the biogenesis of certain specific substrates, such as Tim23 (Leuenberger et al., 1999; Koehler et al., 1999). On the contrary, the human TIM22 complex is 440-kDa protein machinery containing the channel-forming module Tim22 and small Tim chaperones Tim9, Tim10a and Tim10b (functional homolog of yeast Tim12) (Bauer et al., 1999; Mühlenbein et al., 2004; Qi et al., 2021). Furthermore, two additional proteins, Tim29 and AGK, have been identified as novel membrane subunits of the human TIM22 complex (Callegari et al., 2016; Kang et al., 2016, 2017; Vukotic et al., 2017). Despite having subtle changes in the structural composition, the TIM22 complex and its import pathway remain conserved from yeast to higher eukaryotes (Kumar et al., 2022). Importantly, pathological variants in different subunits of the TIM22 complex are identified and implicated in various diseases such as mitochondrial myopathy, Sengers syndrome and Mohr–Tranebjaerg syndrome (deafness–dystonia–optic neuropathy syndrome) (Koehler et al., 1999; Roesch et al., 2002; Kang et al., 2017; Vukotic et al., 2017; Pacheu-Grau et al., 2018). These studies highlight the role of defective mitochondrial protein biogenesis through the TIM22 pathway in neurological and musculoskeletal disease development.

Department of Biochemistry, New Biological Sciences Building, Indian Institute of Science, C V Raman Avenue, Bangalore 560012, India.

*Author for correspondence (patrick@iisc.ac.in)

A.K., 0000-0002-2457-790X; P.D., 0000-0002-1619-5311

Handling Editor: Jennifer Lippincott-Schwartz
Received 29 March 2022; Accepted 13 December 2022

Journal of Cell Science (2023) 136, jcs260060. doi:10.1242/jcs.260060

The model substrates of the TIM22 pathway include the large family of metabolite carrier proteins such as Pic (also referred to as Pic2), Aac2 (also referred to as Pet9) and Dic1, which all have six transmembrane (TM) segments (Endres et al., 1999; Horten et al., 2020). The TIM22 complex also mediates the membrane insertion of specific components of the translocases (Tim17, Tim22 and Tim23) that contain four TM regions (Leuenberger et al., 1999; Horten et al., 2020; Paschen et al., 2000). Recently, mitochondrial pyruvate carriers (MPCs), which possess three TM segments, and sideroflexins (SFXNs), which have five TM regions, were identified as unconventional client proteins of the TIM22 pathway (Gomkale et al., 2020; Rampelt et al., 2020; Acoba et al., 2021; Jackson et al., 2021). The substrates of the TIM22 pathway are highly hydrophobic, and their proper assembly is critical for maintaining mitochondrial proteostasis. Thus, the turnover of these protein substrates needs to be efficient in maintaining mitochondrial homeostasis.

Mitochondrial protein quality control is maintained by multiple mechanisms such as mitochondrial dynamics, mitophagy, proteasome-assisted protein degradation, chaperones and proteases (Ruan et al., 2020; Song et al., 2021). Amongst them, mitochondrial proteases operate at the molecular level and regulate quality control, ensuring a healthy mitochondrial pool (Koppen and Langer, 2007). Yme1 is an IM mitochondrial protease involved in the degradation of misfolded or unfolded IM or intermembrane space proteins, and specific outer membrane (OM) proteins (Leonhard et al., 2000; Gerdes et al., 2012; Wu et al., 2018). It belongs to the i-AAA family of proteases that function in an ATP-dependent manner (Leonhard et al., 1999). Structurally, the YME1 complex encompasses the core component Yme1 and two additional subunits, Mgr1 and Mgr3 (Dunn et al., 2008). Yme1 is a zinc metalloprotease consisting of a protease domain and an ATPase domain that work together for substrate processing, whereas Mgr1 and Mgr3 act as adaptor proteins (Puchades et al., 2017). Yme1 regulates multiple arrays of the proteins, subunits of the electron transport chain such as Cox2 and Cox4, small Tim protein Tim10 and mitophagy-selective receptor Atg32 (Weber et al., 1996; Stiburek et al., 2012; Wang et al., 2013; Spiller et al., 2015). Moreover, the loss of Yme1 results in abnormal mitochondrial morphology and increased frequency of mitochondrial DNA escape (Thorsness et al., 1993; Campbell and Thorsness, 1998; Cesnekova et al., 2018).

In higher eukaryotes, YME1L1, the functional homolog of Yme1, is involved in the cleavage of OPA1, a key regulator of mitochondrial fusion and fission (Griparic et al., 2007; Tilokani et al., 2018). Furthermore, mutations in YME1L1 are associated with optic atrophy (Hartmann et al., 2016). Additionally, Tim17A, a substrate of the TIM22 pathway, was shown to be the degradation substrate of YME1L1, suggesting a possible interplay between quality control and the mitochondrial IM import machinery (Rainbolt et al., 2013). Interestingly, in yeast, Tim54, a membrane subunit of the TIM22 complex, is required to assemble Yme1 into the active proteolytic complex (Hwang et al., 2007). Furthermore, Yme1 was demonstrated to be required for quality control of Aac2 (Liu et al., 2015). Taken together, these findings suggest a possible interplay between the mitochondrial quality and IM import machinery via functional crosstalk between the TIM22 complex and YME1 machinery.

The present study demonstrates a novel functional association between the TIM22 complex and YME1 machinery in *Saccharomyces cerevisiae*. Our genetic, biochemical and cell biological analyses provide compelling evidence to highlight the functional dependence of the TIM22 complex and YME1 machinery in regulating IM protein quality control and, thus, overall mitochondrial health.

RESULTS

Impairment in the TIM22 complex alleviates the respiratory incompetency of cells lacking Yme1

To understand the significance of the TIM22 complex in mitochondrial quality control, we investigated the effect of the impaired TIM22 translocase activity in cells devoid of Yme1. To begin with, we generated single-deletion strains, *tim18*Δ (impaired TIM22 complex) and *yme1*Δ, and a double-deletion strain *tim18*Δ *yme1*Δ in the W303 haploid background. Upon *in vivo* phenotypic analysis, the *tim18*Δ strain showed a similar growth pattern as the wild type (WT) at all the indicated temperatures in yeast extract peptone dextrose (YPD) and yeast extract peptone glycerol (YPG) media (Fig. 1A). On the contrary, the *yme1*Δ strain exhibited severe growth defects at 37°C in YPG and a mild growth sensitivity at 14°C in YPD and YPG media, in agreement with previous reports (Fig. 1A) (Thorsness et al., 1993; Thorsness and Fox, 1993). The disruption of both Tim18 and Yme1 led to slight growth defects at 37°C in YPD medium and 14°C in both YPD and YPG media (Fig. 1A). Strikingly, the *tim18*Δ *yme1*Δ strain displayed better restoration of cellular growth compared to *yme1*Δ cells at 37°C in YPG medium (Fig. 1A). Additionally, when we performed growth-curve analysis at 37°C in YPG medium, the *tim18*Δ *yme1*Δ strain showed a significant growth rescue compared to *yme1*Δ cells (Fig. 1B). The identity of the deletion strains was further validated by immunoblotting analysis (Fig. 1C). Moreover, the complementation of the *tim18*Δ *yme1*Δ strain with a construct expressing Tim18 under its native promoter displayed a severe growth sensitivity at 37°C in non-fermentable medium [synthetic complete glycerol (SCG)–Ura], comparable to *yme1*Δ cells (Fig. 1D). Tim18 protein expression in the *tim18*Δ *yme1*Δ strain was confirmed by immunoblotting (Fig. 1E). Furthermore, we used *tim22* conditional mutants to validate the genetic link between these complexes (Kumar et al., 2020). Interestingly, the deletion of Yme1 in a *tim22* mutant background (*tim22*^{K127A}) exhibited partial rescue in the growth defects of *yme1*Δ at 37°C in YPG medium (Fig. 1F). Taken together, these findings provide genetic evidence for a novel functional link between the TIM22 and YME1 complexes.

Next, we examined whether the rescue of growth defects of *yme1*Δ is specific to Tim18 loss or a consequence of impairment of the TIM22 complex. To address this, Tim18 and Tim22 were overexpressed under the *TEF* promoter and we analyzed their effect on the growth of WT and *yme1*Δ strains by serial dilution assays. Remarkably, the overexpression of Tim22 compromised the growth of cells lacking Yme1 at all tested temperatures in both fermentable [synthetic complete dextrose (SCD)–Ura] and non-fermentable (SCG–Ura) media (Fig. S1A). At the same time, the overexpression of Tim22 did not affect the growth of the control WT strain (Fig. S1A). In contrast, the overexpression of Tim18 did not alter the growth phenotypes of either the WT or *yme1*Δ strains (Fig. S1B). Tim22 and Tim18 protein overexpression were confirmed by immunoblotting (Fig. S1C,D). In conclusion, these results establish that impairment in the TIM22 complex suppresses the respiratory growth defect of cells devoid of Yme1 at elevated temperatures, highlighting an intricate genetic link between the carrier translocase machinery and the YME1 complex.

Association between the TIM22 complex and YME1 machinery is critical for respiration and mitochondrial integrity

To gain insights into the respiratory growth defects of cells lacking Yme1, we first examined the oxygen consumption rate (OCR) in WT and deletion strains at 37°C in YPG medium using a Seahorse

Journal of Cell Science (2023) 136, jcs260060. doi:10.1242/jcs.260060

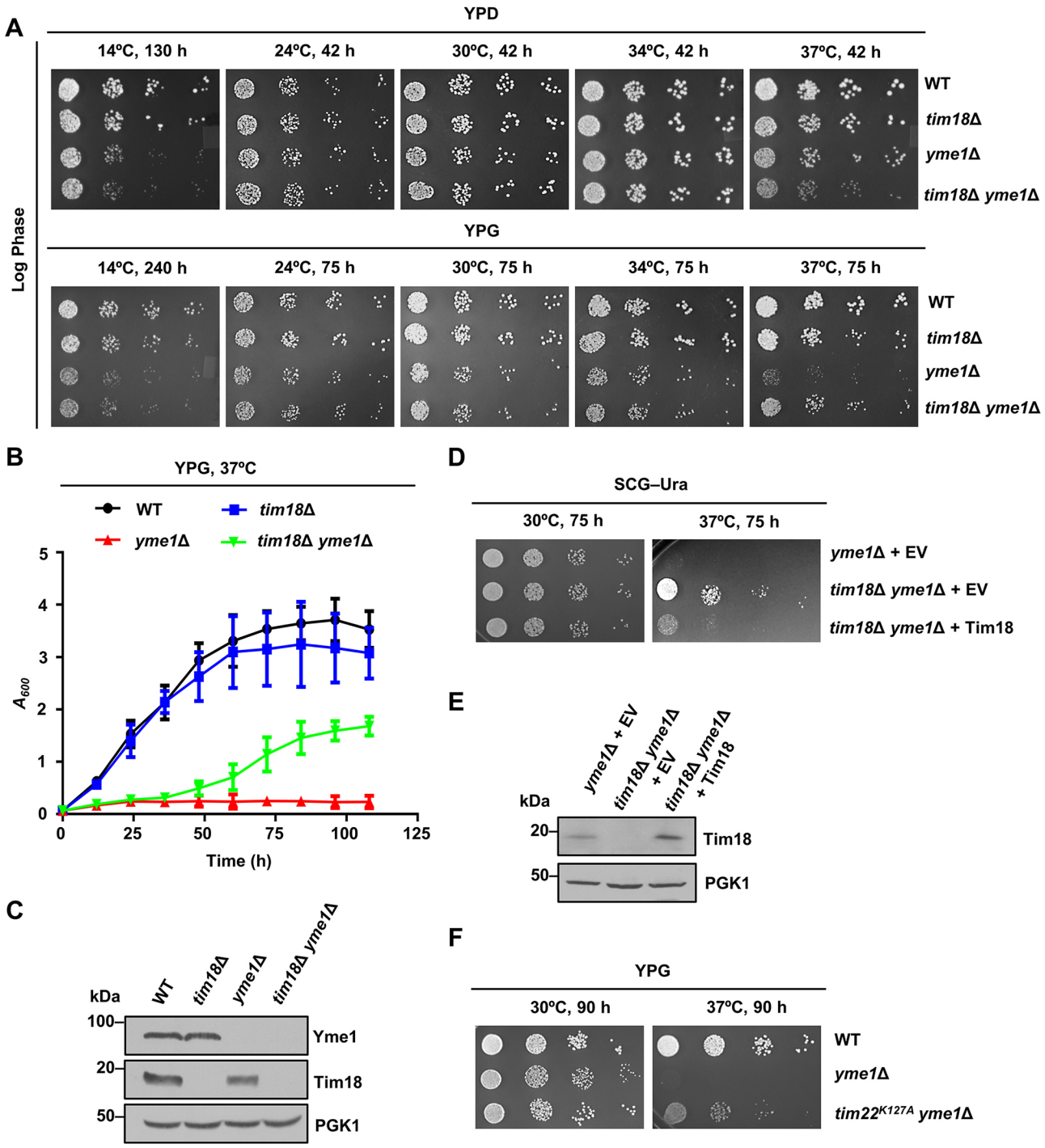

Fig. 1. The impairment in the TIM22 complex rescues the respiratory growth defects of *yme1*Δ cells. (A) Growth phenotype assessment. WT, *tim18*Δ, *yme1*Δ *and tim18*Δ *yme1*Δ yeast strains were allowed to grow up to mid-log in YPD broth at 30°C. Ten-fold serially diluted cells were spotted on the indicated media and incubated at different temperatures. (B) Growth curve analysis. Quantitation of the growth of WT, *tim18*Δ, *yme1*Δ *and tim18*Δ *yme1*Δ yeast strains grown in YPG medium at 37°C. Error bars indicate the mean±s.e.m. of *n*=3 biological replicates. (C) Measurement of steady-state protein levels. Whole-cell extracts of the respective strains were evaluated by immunoblotting. (D) Complementation of the growth phenotype. *yme1*Δ and *tim18*Δ *yme1*Δ strains harboring either an empty vector (EV) or Tim18-expressing plasmid were grown to mid-log phase, serially diluted and spotted on the SCG–Ura medium. (E) Evaluation of Tim18 expression. Steady-state levels of Tim18 were measured in whole-cell extracts by immunoblotting. (F) Growth phenotype analysis. Yeast cells (WT, *yme1*Δ and the *tim22*^{K127A} strain containing a mutation in the TM2 region of Tim22 and lacking Yme1) were grown to mid-log phase, serially diluted and spotted on the YPG medium. The plates were incubated at different temperatures and images were taken at the indicated time intervals. Data in A–F are representative of *n*=3 biological replicates.

XF HS mini analyzer. Upon measurement, WT and *tim18*Δ cells did not show any significant change in the basal respiration rates (Fig. 2A; Fig. S2A). However, the basal OCR was drastically reduced in *yme1*Δ strains, suggesting that loss of Yme1 makes cells incompetent (Fig. 2A; Fig. S2B). Remarkably, the basal OCR was rescued in the *tim18*Δ *yme1*Δ strains, indicating that loss of Tim18

Journal of Cell Science (2023) 136, jcs260060. doi:10.1242/jcs.260060

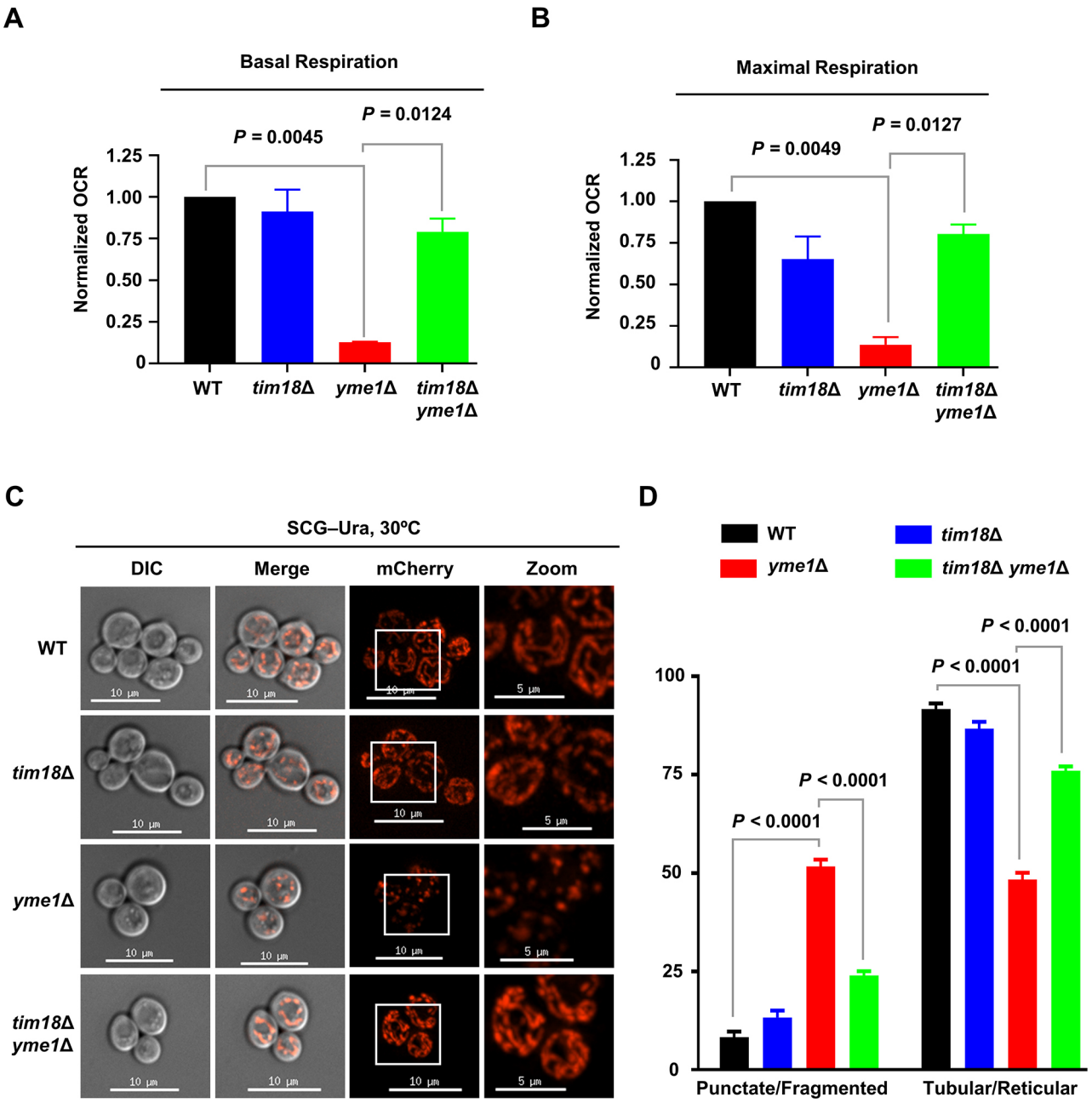

Fig. 2. The loss of Tim18 rescues the respiration and mitochondrial morphology defects of *yme1*Δ cells. (A,B) Evaluation of respiration capacity. An equal number of WT and deletion strains (A_{600}=0.01) were seeded in a poly-D-lysine-coated Seahorse XFp cell culture miniplates to assess OCR. FCCP and rotenone/antimycin A were added one after the other to assess the mitochondrial respiratory states. Basal respiration was calculated as an average of the last OCR before the first FCCP addition subtracted by non-mitochondrial respiration capacity. Maximal respiration was measured as an average of the last OCR following the FCCP injection subtracted by non-mitochondrial respiration capacity. The non-mitochondrial respiration was calculated as an average of the last OCR after rotenone/antimycin A treatment. The fold change in basal and maximal OCRs for the indicated deletion strains was calculated in comparison to WT and plotted as a bar graph. Data represent mean±s.e.m. of *n*=2 biological replicates with three technical replicates. Statistical significance was calculated using one-way ANOVA with Tukey's multiple-comparisons test. The representative graphs showing OCRs for WT and the deletion strains are shown in Fig. S2A–C. (C,D) Assessment of mitochondrial morphology. Yeast strains (WT, *tim18*Δ, *yme1*Δ and *tim18*Δ *yme1*Δ) expressing an MTS–mCherry construct were subjected to microscopic analysis for the visualization of mitochondria. The images in all the panels were captured at identical exposures and the mitochondrial structures from ≥50 cells were assessed using SoftWoRx 6.1.3 software. Boxes indicate the magnified regions shown in the zoomed panels. Error bars in the graphs represent the mean±s.e.m. in the percentage of the population. Scale bars: 10 µm and 5 µm (zoom). The data shown above are representative of *n*=3 individual experiments. Statistical significance was calculated using two-way ANOVA with Tukey's multiple-comparisons test.

mitigates the respiratory incompetency of cells devoid of Yme1 (Fig. 2A; Fig. S2C). Additionally, we analyzed the maximal respiration capacity of the WT and deletion strains after treatment with carbonyl cyanide-*p*-trifluoromethoxyphenylhydrazone (FCCP), a mitochondrial oxidative phosphorylation uncoupler. Upon quantification, we observed that WT and *tim18*Δ cells exhibited comparable maximal respiration rates (Fig. 2B; Fig. S2A). Conversely, *yme1*Δ strains showed severe impairment in the

Journal of Cell Science (2023) 136, jcs260060. doi:10.1242/jcs.260060

maximum respiration capacity (Fig. 2B; Fig. S2B). Notably, the maximal respiration rate was significantly rescued in *tim18*Δ *yme1*Δ cells (Fig. 2B; Fig. S2C).

We next analyzed mitochondrial structures, as defective respiration is an indication of impaired mitochondrial integrity. As the deletion of Tim18 rescued the growth of *yme1*Δ cells (*tim18*Δ *yme1*Δ) in respiratory medium, we hypothesized that a possible reversal of mitochondrial integrity could occur through productive, functional crosstalk between the TIM22 and YME1 complexes. To validate this hypothesis, the mitochondrial morphology of WT, *tim18*Δ, *yme1*Δ and *tim18*Δ *yme1*Δ strains was examined by microscopy. The mitochondrial network was visualized using the MTS–mCherry construct, which exclusively decorates mitochondria. WT and deletion strains expressing MTS–mCherry were grown in glycerol-containing medium at the permissive temperature, and mitochondrial morphology was monitored by fluorescence imaging. Most of the WT and *tim18*Δ cells displayed a reticular or tubular mitochondrial network (Fig. 2C,D). However, the *yme1*Δ strain demonstrated fragmented or punctate mitochondrial structures (Fig. 2C,D), in agreement with previous findings (Campbell and Thorsness, 1998; Campbell et al., 1994). Interestingly, *tim18*Δ *yme1*Δ cells showed enrichment of reticular or tubular mitochondrial networks, suggesting that the deletion of Tim18 can rescue the mitochondrial morphological defects associated with *yme1*Δ cells under respiratory growth conditions (Fig. 2C,D). Taken together, these results suggest that functional interplay between the TIM22 and YME1 complexes is crucial for mitochondrial integrity and cellular respiration.

Crosstalk between the TIM22 complex and YME1 machinery maintains mitochondrial functions

To further delineate the importance of the genetic link between the TIM22 and YME1 complexes in mitochondrial health, we examined different mitochondrial functional parameters. *YME1* was identified in a genetic screen for isolating genes that manifest an increased frequency of mitochondrial DNA migration to the nucleus (Thorsness and Fox, 1993). We assessed mitochondrial DNA stability as one of the parameters to evaluate mitochondrial health. We used a genetic approach to examine where the nuclear *TRP1* gene, including its regulatory regions, was integrated into the mitochondrial genome in a strain lacking its endogenous *TRP1* gene (Fig. 3A) (Thorsness et al., 1993). The mitochondrial *TRP1* gene, when migrated to the nucleus, becomes functional as the required transcription machinery is only present in the nucleus. The presence of *TRP1* in mitochondrial DNA permits monitoring of the rate at which mitochondrial DNA fragments escape from the organelle. Upon assessment, the *yme1*Δ strain demonstrated higher mitochondrial DNA transfer frequency in a time-dependent manner consistent with earlier findings (Fig. 3B,C) (Thorsness et al., 1993; Cheng and Ivessa, 2010). However, the *tim18*Δ *yme1*Δ strain showed mitochondrial DNA transfer frequency comparable to the WT and *tim18*Δ strains, indicating that loss of Tim18 reduces the mitochondrial DNA escape frequency of cells devoid of Yme1 (Fig. 3B,C). As a loading control, an equal number of cells from the WT and deletion strains were serially diluted and spotted on YPD medium (Fig. 3D). To further corroborate the above result, we checked for mitochondrial DNA content using the mitochondrial DNA-specific dye SYTO 18. The WT and deletion strains were grown in YPG medium under permissive conditions, followed by staining with SYTO 18 and visualization by fluorescence imaging. Strikingly, the *yme1*Δ strain displayed reduced levels of SYTO 18 fluorescence than WT and *tim18*Δ strains (Fig. 3E). In contrast, the *tim18*Δ *yme1*Δ strain exhibited SYTO 18 fluorescence levels comparable to those of the WT and *tim18*Δ strains, implying that the deletion of Tim18 decreases the mitochondrial DNA loss frequency of cells deficient in Yme1 (Fig. 3E).

We measured the ATP levels as another criterion for mitochondrial function in deletion strains to validate the above results. Upon evaluation, the levels of mitochondrial ATP were drastically reduced in *yme1*Δ cells compared to WT and *tim18*Δ cells (Fig. 3F). On the contrary, the deletion of Tim18 partially restored the ATP levels in cells lacking Yme1, indicating that the growth defects of the *yme1*Δ cells in respiratory medium are a consequence of the impairment in mitochondrial functions (Fig. 3F). Porin (Por1), an OM protein, was used as a control to ensure that equal amounts of mitochondria were used for the analysis (Fig. 3F). Collectively, these findings signify that the functional link between the TIM22 complex and YME1 machinery plays an essential role in conserving mitochondrial functions.

Yme1 is critical for regulating the proteostasis of TIM22 pathway substrates

To get mechanistic insights into the significance of the association between the TIM22 complex and YME1 machinery, we analyzed the steady-state protein levels of TIM22 pathway substrates in the cellular lysates of the WT and deletion strains grown in YPG medium at the permissive temperature. The protein levels of Dic1, Aac2 and Tim23 were observed to be similar between WT and *tim18*Δ strains (Fig. 4A,B). However, the *yme1*Δ strain showed higher levels of Dic1, Aac2 and Tim23 than the WT strain (Fig. 4A,B). Remarkably, the levels of these proteins were significantly reduced in the *tim18*Δ *yme1*Δ strain compared to the *yme1*Δ strain (Fig. 4A,B). As controls, the levels of Por1 and PGK1 remained unaltered in the WT and all the deletion strains (Fig. 4A,B). To delineate the functional coordination of the TIM22 pathway and YME1 machinery at the organellar level, the steady-state expression of TIM22 complex substrates was analyzed from isolated mitochondrial lysates. Interestingly, the mitochondrial levels of Dic1, Aac2 and Tim23 were comparable between WT and all the deletion strains, indicating that the absence of Yme1 results in the accumulation of these proteins outside the mitochondria (Fig. 4C,D).

We next checked whether the growth impairment of *yme1*Δ cells was due to the enhanced levels of TIM22 substrates, in which case overexpression of these cargos would aggravate the growth sensitivity of *yme1*Δ cells. To test the hypothesis, metabolite carrier proteins (Pic, Aac2 and Dic1) and Tim23 were overexpressed, followed by growth phenotype analysis. The overexpression of Dic1 did not affect the growth of WT and *tim18*Δ cells compared to the *yme1*Δ strain, which exhibited severe growth defects at all temperatures in fermentable medium (SCD–Trp) (Fig. 5A). Additionally, *tim18*Δ *yme1*Δ cells showed severe growth defects upon Dic1 overexpression under the same experimental conditions (Fig. 5A). This signifies that the activity of carrier translocase and protease systems is crucial for handling the excess TIM22 pathway substrates. The overexpression of Dic1 was confirmed by immunoblotting (Fig. 5B). Similarly, the overexpression of Tim23 considerably impaired the growth of the *yme1*Δ strain at 37°C and further enhanced the growth defects of the *tim18*Δ *yme1*Δ strain at all tested temperatures in fermentable medium (SCD–Trp) (Fig. S3A). The overexpressed Tim23 protein levels were validated by immunoblotting in WT and deletion strains (Fig. S3B). Moreover, the overexpression of more complex cargo proteins such as Pic and Aac2 resulted in the lethality of *yme1*Δ and

Journal of Cell Science (2023) 136, jcs260060. doi:10.1242/jcs.260060

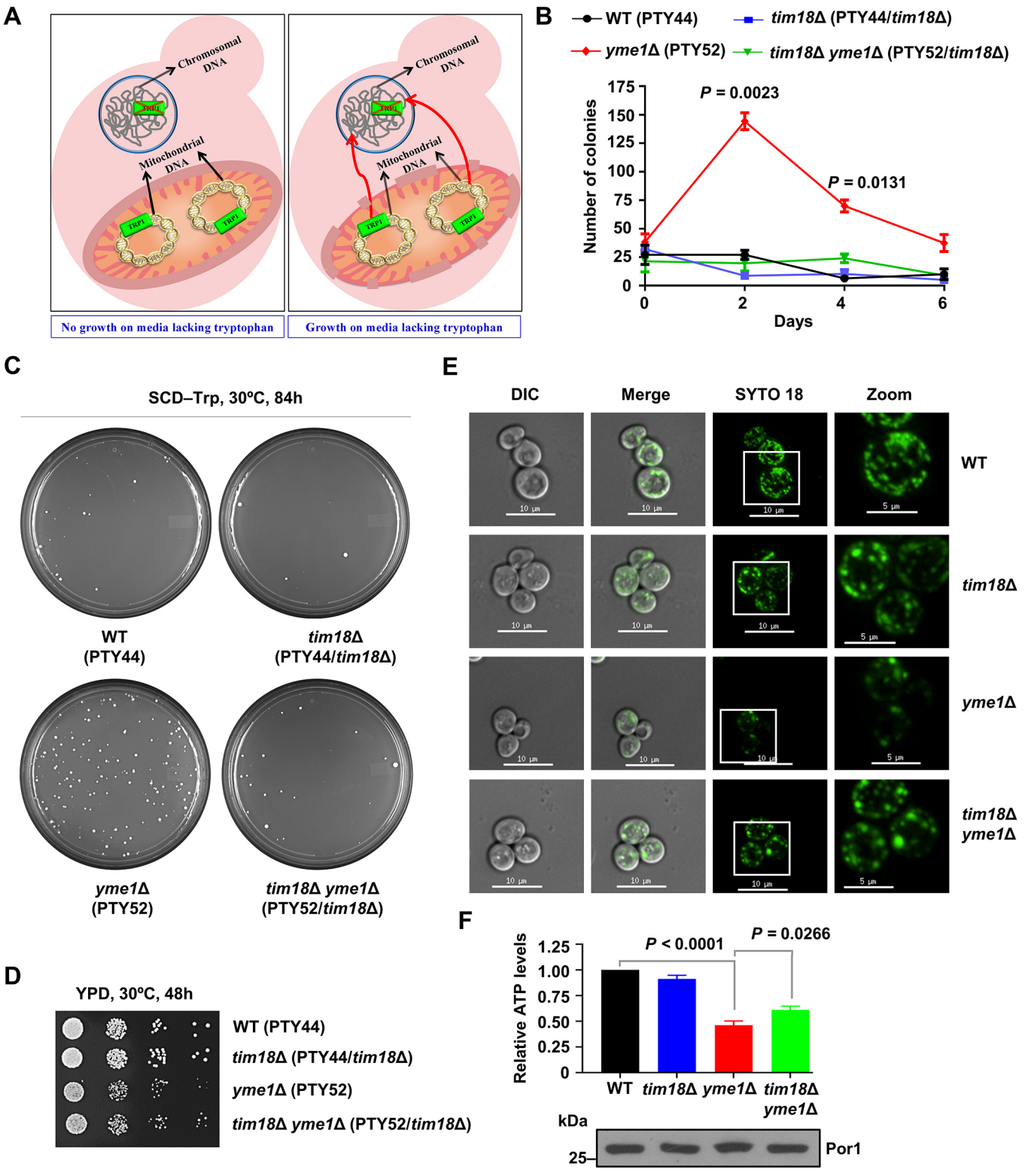

Fig. 3. See next page for legend.

*tim18*Δ *yme1*Δ cells (Fig. S3C,D). As a control, the overexpression of an OM protein, Tom6, or a matrix protein, Abf2, did not alter the growth of either WT or any deletion strains under similar experimental conditions (Fig. S3E,F). Furthermore, the overexpression of Tim18 (an IM protein and substrate of the TIM23 pathway) did not affect the growth phenotype of cells lacking Yme1 (Fig. S1B,D), suggesting that the growth defect of the *yme1*Δ strain is a consequence of impairment in the TIM22 pathway.

To check whether higher levels of TIM22 pathway substrates influence mitochondrial integrity and thus further impair the cellular growth of *yme1*Δ cells, we examined the mitochondrial morphology in Dic1-overexpressing cells grown in fermentable

Journal of Cell Science (2023) 136, jcs260060. doi:10.1242/jcs.260060

Fig. 3. The deletion of Tim18 restores the functional mitochondrial parameters in *yme1*Δ cells. (A) Schematic representation of a genetic assay to determine the rate of mitochondrial DNA migration. The endogenous nuclear yeast *TRP1* gene is deleted from the genome and is inserted into mitochondrial DNA. The *TRP1* gene gets functional after it migrates from mitochondria to the nucleus as the required transcription machinery is only present in the nucleus. The migration of the *TRP1* gene from mitochondria to the nucleus allows cells to grow on medium lacking the amino acid tryptophan. (B) Estimation of mitochondrial DNA transfer frequency. The mitochondrial DNA transmission frequency was determined by plating an equal number of cells (A_{600}=0.5) on medium deprived of tryptophan, followed by calculating the number of colonies obtained at different time intervals and represented as mean±s.e.m. of *n*=3 biological replicates. Significance testing was performed using two-way ANOVA with Tukey's multiple-comparisons test. (C) A representative image demonstrating the number of colonies in different strains on day 2 is shown. (D) WT and deletion strains were serially diluted and spotted on YPD medium. (E) Mitochondrial DNA content analysis by fluorescence microscopy. Yeast cells grown up to the mid-log phase were stained with 10 µM SYTO 18 for 15 min, followed by mitochondrial DNA visualization using fluorescence microscopy. The images were captured by keeping all the microscopic parameters constant and analyzed using SoftWoRx 6.1.3 software. Scale bars: 10 µm and 5 µm (zoom). (F) Measurement of mitochondrial ATP levels. 50 µg mitochondria isolated from the indicated strains were lysed and analyzed by the ATP detection reagent from the Mitochondrial ToxGlo Assay kit. Porin (Por1) was used as a loading control. The relative ATP levels were quantitated by calculating the fold change and represented as a bar graph. Error bars indicate the mean±s.e.m. of *n*=3 biological replicates. One-way ANOVA with Tukey's multiple-comparisons test was used for calculating statistical significance.

medium at the permissive temperature. Intriguingly, WT cells overexpressing Dic1 retained their tubular mitochondrial network, whereas the *yme1*Δ strain overexpressing Dic1 demonstrated further enhancement in mitochondrial fragmentation even under fermentable growth conditions at the permissive temperature, implying that excess levels of TIM22 pathway substrates impair mitochondrial integrity in the absence of Yme1 (Fig. 5C,D).

A previous finding reported that partial suppression of cytosolic protein synthesis rescues the cellular lethality of *yme1*Δ cells expressing a pathogenic variant of Aac2 (Wang et al., 2008). To determine whether loss of Tim18 can rescue the growth defects of cells lacking Yme1 following a similar mechanism, we performed the growth assessment of WT, *yme1*Δ and *tim18*Δ *yme1*Δ after cycloheximide (CYH) treatment. Strikingly, CYH treatment did not change the growth pattern of any of the strains compared to untreated cells under our experimental conditions (Fig. 5E). Cytoplasmic protein synthesis inhibition upon CYH treatment was ascertained by performing immunoblot analysis against several cytoplasmic proteins. As indicated in Fig. S4A,B, a reduction in the steady-state levels of cytosolic proteins such as Ydj1, Hsp31 and SOD1 was observed in the deleted strains upon CYH treatment. These results further highlight that the partial suppression of cytoplasmic protein synthesis does not rescue the growth defects of cells lacking Yme1 under respiratory growth conditions. Additionally, the levels of Ssb1 remained unaltered in WT and all the deletion strains at both 30°C and 37°C (Fig. S4C,D). Ssb1 is a cytoplasmic chaperone that regulates the accumulation of proteins in the cytosol and is upregulated in *tim18*Δ cells lacking mitochondrial DNA (Dunn and Jensen, 2003; Wang and Chen, 2015). Hence, these findings suggest a possible involvement of a novel cellular response associated with the TIM22 pathway and YME1 machinery. In summary, these results suggest that excess protein levels of TIM22 pathway substrates impair mitochondrial integrity, thus leading to the growth sensitivity of cells deprived of Yme1 under respiratory conditions. However, compromising the TIM22 pathway in cells lacking Yme1 preserves mitochondrial morphology and functions, possibly by reducing the levels of TIM22 pathway substrates, leading to cellular growth rescue.

Yme1 is required for the stability of the TIM22 complex

To dissect the functional link between the TIM22 complex and YME1 protease machinery, we next estimated the steady-state protein levels of different components of the carrier translocase machinery and Yme1 in isolated mitochondria from WT and deletion strains grown in non-fermentable medium. Upon analysis, we found a slight reduction in Tim22 protein levels in the mitochondrial lysates of the *tim18*Δ strain at both 30°C and 37°C compared to those from the WT strain (Fig. S5A; Fig. 6A). This agrees with previous findings in which Tim18 was demonstrated to be involved in maintaining Tim22 stability (Koehler et al., 2000; Kerscher et al., 2000). Furthermore, the levels of Tim22 and Tim18 were marginally reduced in *yme1*Δ cells at 30°C (Fig. S5A). Strikingly, the levels of Tim22 and Tim18 were significantly reduced together with a minor decline in the levels of Tim54 in cells lacking Yme1 at 37°C (Fig. 6A). Additionally, the *tim18*Δ *yme1*Δ strain showed a reduction in Tim22 levels at 30°C, whereas the levels of Tim54 and Tim22 were significantly decreased at 37°C (Fig. S5A; Fig. 6A). On the contrary, the levels of Yme1 protein were comparable between the WT and *tim18*Δ strains at both 30°C and 37°C (Fig. S5A; Fig. 6A). As positive controls, the amounts of porin and Tim50 (a marker for the IM) were examined and found to be comparable between WT and all the deletion strains (Fig. S5A; Fig. 6A). These results suggest that the loss of Yme1 alters the steady-state levels of different subunits of the TIM22 complex, especially at elevated temperatures.

We further investigated the effect of Yme1 deletion on the stability of the TIM22 complex using Coomassie Blue-stained native PAGE (BN-PAGE). The WT mitochondria isolated from cells grown at 30°C in YPG medium displayed a stable TIM22 complex at ∼300 kDa when immunodecorated with antibodies specific for Tim54 and Tim22 (Fig. 6B). On the contrary, mitochondria isolated from *tim18*Δ and *tim18*Δ *yme1*Δ strains exhibited destabilization of the TIM22 complex (Fig. 6B). This finding agrees with earlier reports in which the loss of Tim18 was shown to impair the architecture of the TIM22 complex (Koehler et al., 2000; Kerscher et al., 2000). Surprisingly, the levels of the 300-kDa TIM22 complex were significantly affected in cells devoid of Yme1 (Fig. 6B). Furthermore, the stability of the TIM22 complex was more drastically affected at 37°C in Yme1-deficient cells (Fig. S5B). This correlates well with the reduction in the levels of Tim22 and Tim18 shown above. On the contrary, the levels of the YME1 complex remained unaffected between the WT and *tim18*Δ strains, suggesting that loss of Tim18 does not affect the stability of the YME1 complex (Fig. 6B). As a control, the amounts of the porin complex were assessed and found to be comparable between WT and all the deletion strains at 30°C and 37°C (Fig. 6B; Fig. S5B). Taken together, these results highlight that the deletion of Yme1 affects the stability of the TIM22 complex.

To gain more insight into the connection between these systems, we next assessed whether the TIM22 and YME1 complexes physically interact with each other. To test this, we isolated mitochondria from WT cells and strains expressing C-terminally FLAG-tagged Tim18 and subjected them to co-immunoprecipitation (co-IP) using anti-FLAG prebound to protein G sepharose beads. Upon analysis, Tim18–FLAG efficiently immunoprecipitated Tim54 and Sdh3 (Fig. 6C),

Journal of Cell Science (2023) 136, jcs260060. doi:10.1242/jcs.260060

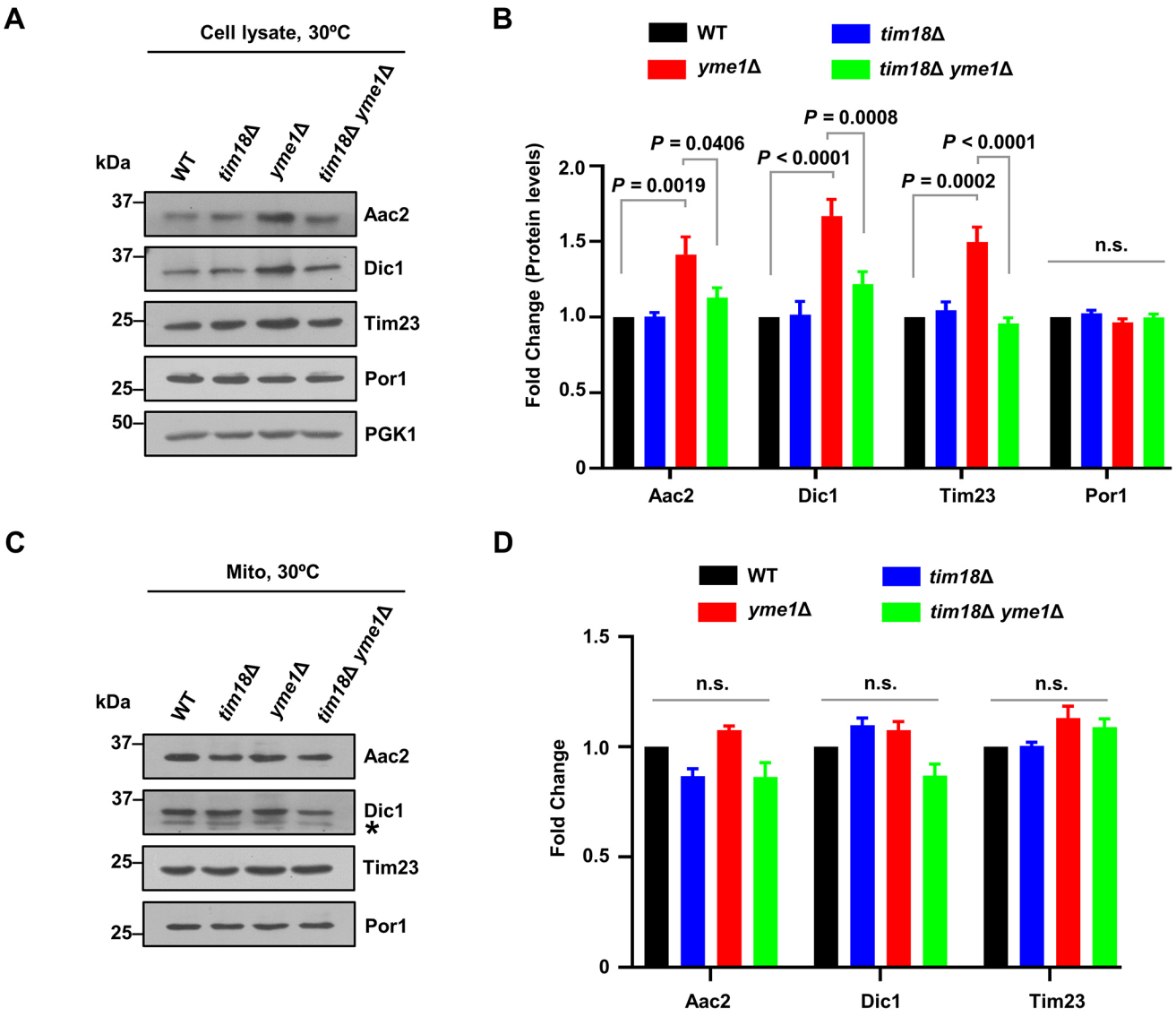

Fig. 4. Cells lacking Yme1 exhibit excess levels of the TIM22 pathway substrates. (A–D) Analysis of steady-state protein levels of the carrier translocase machinery substrates. The protein levels of TIM22 pathway cargos were estimated in the whole-cell lysates and mitochondria of WT and deletion strains grown in YPG at 30°C by immunoblotting. The asterisk specifies the presence of a non-specific band. The protein bands were quantified using ImageJ software and plotted as fold change compared to WT protein levels. Data represent mean±s.e.m. of *n*=3 biological replicates. Statistical significance was calculated using two-way ANOVA with Tukey's multiple-comparisons test. n.s., not significant.

corroborating with a previous report (Kumar et al., 2020). Intriguingly, we observed co-purification of Yme1 along with Tim18–FLAG (Fig. 6C). Tim44, a subunit of the TIM23 complex, and mitochondrial lysates from WT cells were used as negative controls to determine the specificity (Fig. 6C). Furthermore, we performed a similar co-IP with strains expressing either C-terminally FLAG-tagged Tim23 or SOD1. Interestingly, both Tim23–FLAG and SOD1–FLAG failed to immunoprecipitate Yme1, ruling out the possibility of a FLAG-specific interaction of Yme1 (Fig. 6D,E). Based on these findings, we envisioned that the TIM22 complex and YME1 machinery are in proximity to each other in the mitochondrial IM.

DISCUSSION

The current study highlights a functional interplay of the TIM22 complex and YME1 protease machinery in regulating mitochondrial health and integrity (Fig. 7). Our genetic analyses indicate that the deletion of Tim18, a membrane component of the TIM22 complex, rescues the respiratory growth defects of cells devoid of Yme1. Additionally, one of the mutations in the TM2 region of Tim22 (*tim22*^{K127A}) partially suppresses the growth defects of cells lacking Yme1 under respiratory conditions. Furthermore, by utilizing protein overexpression, biochemical and cell biological studies, we demonstrated that the growth rescue of cells deprived of Yme1 is a consequence of impairment in the TIM22 pathway.

The TIM22 complex is one of the major protein translocases that performs a critical function in the biogenesis of the most intricate polytopic proteins of the mitochondrial IM. However, our understanding regarding the protein homeostasis of the carrier translocase substrates is limited mainly because of a lack of studies related to the regulation of protein turnover under normal and pathological conditions. Therefore, even though the mutations in the various subunits of the TIM22 pathway are known to cause neurological disorders, the underlying mechanisms by which the

Journal of Cell Science (2023) 136, jcs260060. doi:10.1242/jcs.260060

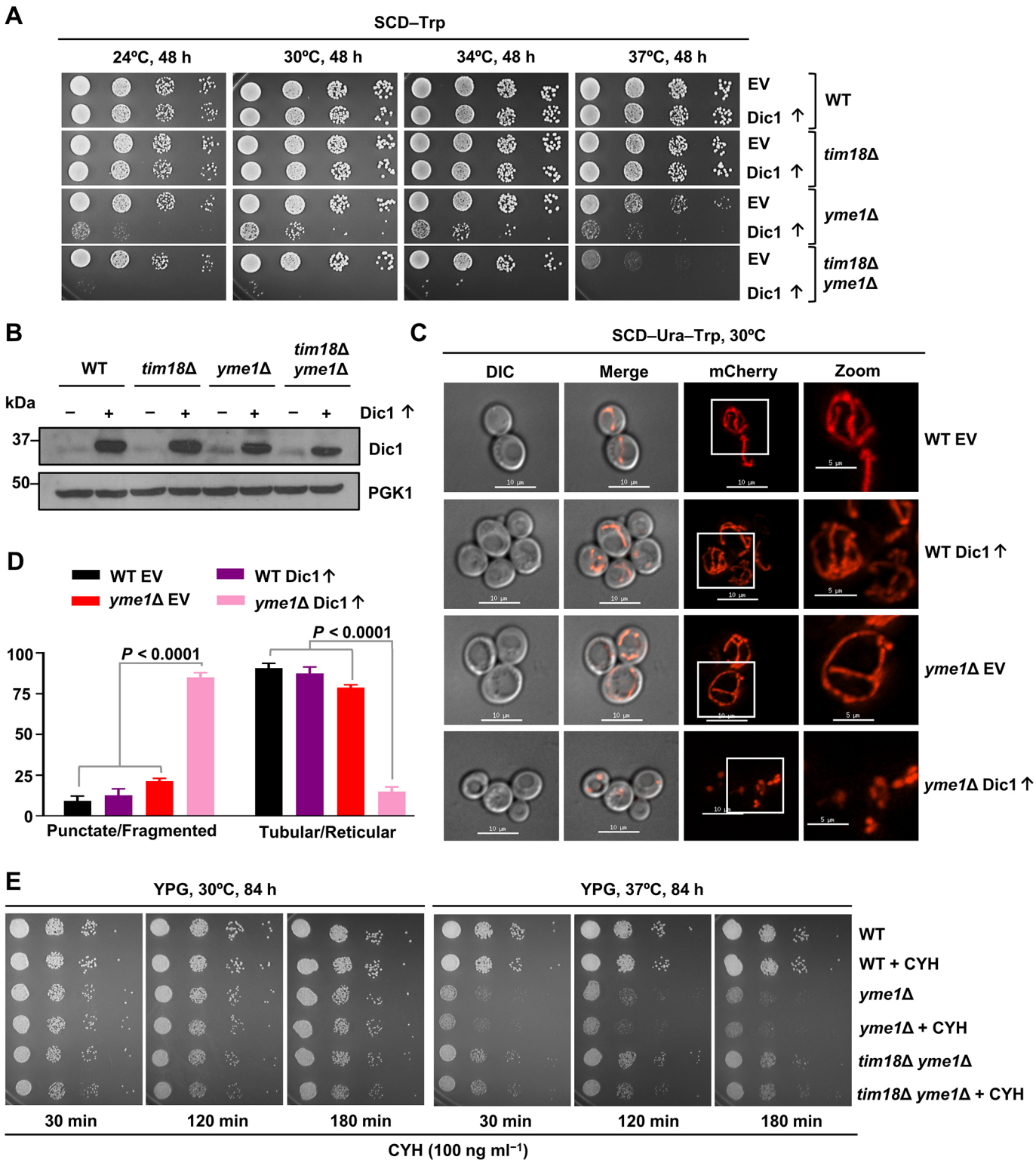

Fig. 5. See next page for legend.

levels of carrier translocase substrates are regulated under such conditions remain enigmatic.

One of the mechanisms by which cells modulate organelle health is by the action of various proteolytic machinery. Yme1 is an i-AAA mitoprotease that plays a crucial role in mitochondrial quality control by regulating the turnover of several membrane proteins. Although Yme1 is vital for mitochondrial protein turnover, cells have evolved with different adaptative mechanisms to survive in the event of its impairment or absence. Previous studies report mutations in the 26S protease subunit and γ subunit of mitochondrial ATP synthase to repress the mitochondrial function and growth defects of *yme1*Δ cells without mitochondrial DNA

Journal of Cell Science (2023) 136, jcs260060. doi:10.1242/jcs.260060

Fig. 5. The overexpression of the TIM22 pathway substrates exacerbates the growth and mitochondrial morphology defects of the *yme1*Δ cells. (A) Growth phenotype examination upon overexpression of Dic1. WT and deletion strains overexpressing Dic1 under the control of centromeric plasmid pRS414$_{TEF}$ were serially diluted, followed by spotting on the indicated medium. (B) Evaluation of Dic1 overexpression. The overexpression of Dic1 was measured by western blotting in whole-cell extracts of the indicated strains. (C,D) Analysis of mitochondrial morphology upon Dic1 overexpression. WT and deletion strains containing MTS–mCherry and Dic1 overexpression constructs were grown to the mid-log phase in YPD at 30°C, and the mitochondrial morphology was visualized using fluorescence microscopy. The microscopic images in all the panels were taken at identical exposures, and the mitochondrial structures from ≥50 cells were assessed using SoftWoRx 6.1.3 software. Boxes depict the magnified regions demonstrated in the zoomed panels. Error bars in the graphs indicate the mean±s.e.m. in the percentage of the population. Scale bars: 10 µm and 5 µm (zoom). Statistical significance was calculated using two-way ANOVA with Tukey's multiple-comparisons test. (E) *In vivo* phenotypic assessment upon CYH treatment. WT, *yme1*Δ *and tim18*Δ *yme1*Δ strains were treated with CYH (100 ng ml^{-1}) for different time intervals, followed by serial dilution and spotting on YPG. The data shown above are from *n*=3 individual experiments.

(Campbell et al., 1994; Weber et al., 1995). Another study revealed that partial inhibition of cytosolic protein synthesis rescues the synthetic lethality of cells lacking Yme1 along with a pathogenic variant of Aac2 (Wang et al., 2008). In a similar line, our study highlights that the impairment in the TIM22 complex promoted the survival of Yme1-deficient cells by rescuing mitochondrial health.

The physiological relevance of the association between import and protease machinery in regulating organellar health

The dynamic association of protein translocases with other mitochondrial components plays a crucial role in modulating organelle homeostasis. For example, the TIM22 complex associates with porin (also known as VDAC) and the mitochondrial contact site and cristae-organizing system (MICOS) complex to facilitate carrier protein biogenesis (Callegari et al., 2019; Ellenrieder et al., 2019). On the contrary, the TIM23 complex coordinates with the respiratory complex to maintain the optimum IM potential required for the protein import (Wiedemann et al., 2007; Matta et al., 2020). In agreement, our finding demonstrates similar coordination between the TIM22 complex and YME1 machinery being in proximity to each other to maintain mitochondrial proteostasis and organelle quality control. Notably, the interaction between carrier translocase machinery and the YME1 complex is transient as Yme1 interacts with Tim18–FLAG in a non-stoichiometric manner, as observed in the co-IP. We believe that a small portion of YME1 machinery is associated with the TIM22 complex, giving rise to different pools of protease machinery to manage diverse substrates. At the organelle level, the loss of Yme1 results in punctate mitochondrial structures, enhanced mitochondrial DNA transfer and compromised respiration capacity, which can be suppressed by altering the TIM22 translocase activity. Hence, it is not unreasonable to believe that the IM proteostasis machinery plays a crucial role in the turnover of misassembled proteins in close connection with import machinery.

Crosstalk between the import and protease machinery regulates IM protein quality control

Previous studies highlight that cells regulate the health of mitochondria by numerous mechanisms, including modulating the components involved in biogenesis and protein translocation rate to avoid the accumulation of misfolded proteins within the organelle. For example, degradation of Tim17A by YME1L1 in higher eukaryotes limits protein import efficiency, thereby assisting mitochondrial proteostasis in response to stress-regulated translation attenuation (Rainbolt et al., 2013). Interestingly, our study provides evidence to show that Yme1 is required for maintaining the stability of the TIM22 complex. We hypothesize that this might be an adaptive strategy to regulate IM protein content due to the unavailability of Yme1. Our study provides compelling evidence that in the absence of Yme1, even though the cells harbored a higher load of substrates due to partial destabilization of the TIM22 complex, the deletion of Tim18 resulted in the relieving the excess of the mitochondrial protein burden, leading to cell survival.

Mitochondrial dysfunction is associated with several pathological states; hence, cells have evolved multiple stress-regulated pathways to maintain mitochondrial proteostasis and organelle function. As the TIM22 pathway substrates are IM proteins with multiple TM segments, any impairment in the TIM22 complex functionality might lead to the accumulation of these highly hydrophobic substrates. Several studies have shown that the accumulation of mitochondrial proteins in the cytosol results in diverse cellular stress responses, such as mitochondrial precursor overaccumulation stress, mitochondrial unfolded protein response, unfolded protein response triggered by mistargeting of proteins, integrated stress response and mitochondrial compromised protein import response (Wang and Chen, 2015; Wrobel et al., 2015; Coyne and Chen, 2018; Weidberg and Amon, 2018). Such stress responses are implicated in several pathological conditions such as aging, muscle degeneration and neurodegeneration (Lin and Beal, 2006; Tatsuta and Langer, 2008; Zhu et al., 2021). In addition, the accumulation of these hydrophobic proteins in the cytosol further dampens the import of other essential cytosolic and mitochondrial proteins (Coyne and Chen, 2019). Additionally, overloading of the carrier proteins in humans induces cytosolic aggresomes and activates apoptotic pathways (Liu et al., 2019). Intriguingly, in our study, *yme1*Δ cells displayed higher levels of the substrates of the TIM22 pathway outside the mitochondria, possibly in the cytosol. Additionally, the loss of Tim18 in the *yme1*Δ strain reduced the accumulation of TIM22 pathway cargos, thereby ensuring cell survival. Further studies are required to identify the stress response pathway in the cells lacking Yme1 and Tim18 to gain mechanistic insights into the mitochondrial quality control mediated by the association of these two complexes.

In summary, the present study revealed a unique functional link between the TIM22 pathway and YME1 machinery in maintaining mitochondrial proteostasis and integrity. Thus, our results provide a primary platform to explore the connection between these two complexes in higher eukaryotes which can be crucial in understanding the pathogenesis of several diseases.

MATERIALS AND METHODS

Yeast strains and genetic manipulations

The yeast strains used in this study are mentioned in Table S1 (Thorsness et al., 1993, Hines et al., 2011, Okamoto et al., 2014). The details of plasmids and primers used in this study are described in Table S2. The *tim18*Δ and *yme1*Δ strains were generated by PCR-mediated homologous recombination to substitute the ORFs with a *kanMX4* and *hphNT1* selection cassette, respectively, in a W303 haploid background. The *tim18*Δ *yme1*Δ strain was created by deleting *YME1*, as mentioned above, in a *tim18*Δ strain. The PTY44/*tim18*Δ and PTY52/*tim18*Δ strains were made by removing *TIM18* in PTY44 and PTY52 strains following a similar approach described above. The WT *TIM18* gene from positions −700 to +859 was PCR amplified from W303 yeast genomic DNA for complementation studies.

Journal of Cell Science (2023) 136, jcs260060. doi:10.1242/jcs.260060

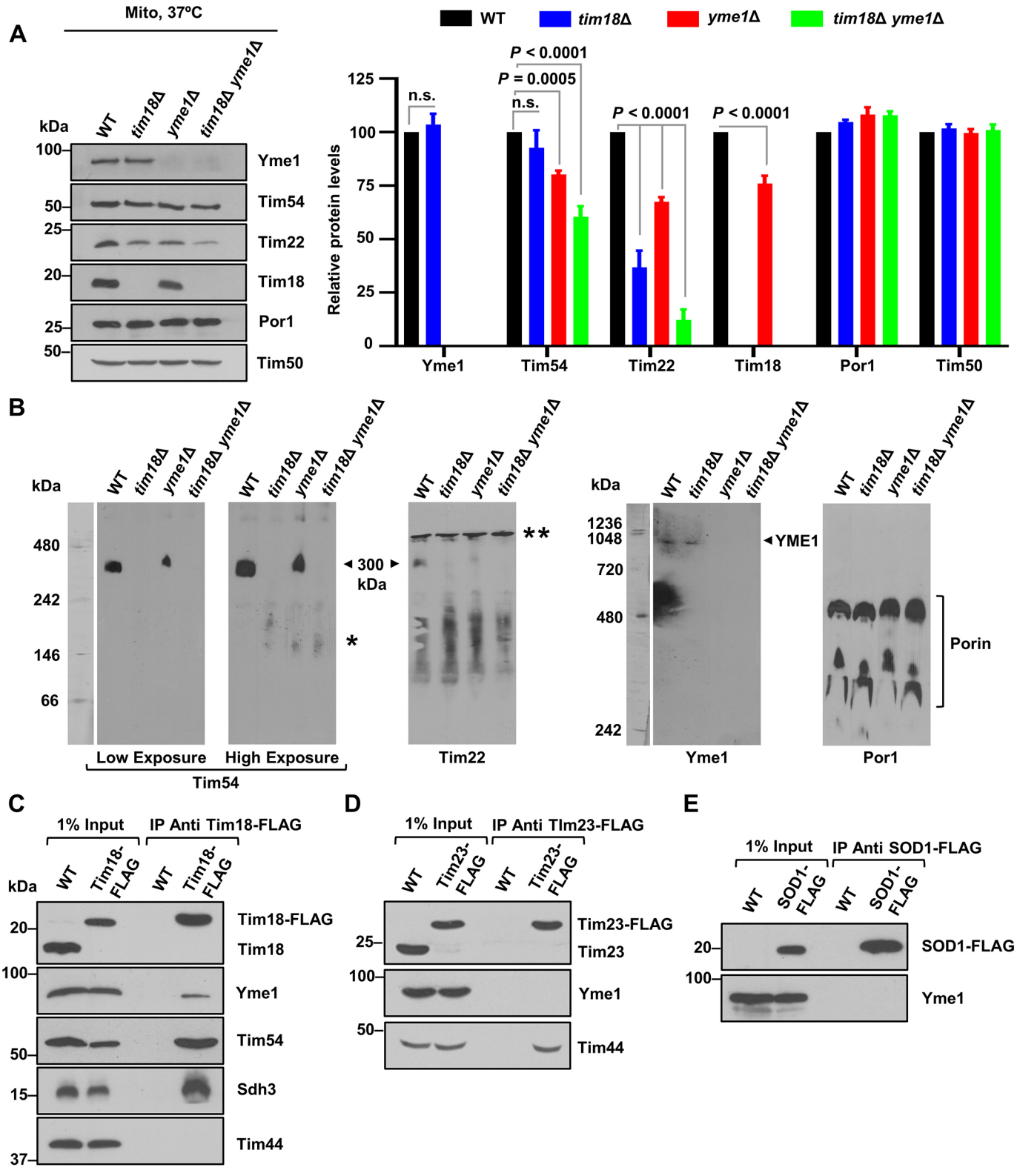

Fig. 6. See next page for legend.

The PCR-amplified products were cloned into the NotI/SalI-digested yeast centromeric vector pRS316 (plasmid gifted by Prof. Elizabeth A. Craig, University of Wisconsin-Madison, USA). For overexpression of Pic, Aac2, Dic1, Tim23, Abf2 and Tom6, the corresponding open reading frames were PCR amplified from yeast genomic DNA and cloned into the pRS414$_{TEF}$ vector (plasmid gifted by Prof. Elizabeth A. Craig). The *TIM22* gene was PCR amplified from yeast genomic DNA and cloned into the pRS416$_{TEF}$ vector (plasmid gifted by Prof. Elizabeth A. Craig) for overexpression experiments. The Tim22 mutant and other overexpression constructs used in this study are described in detail in an earlier report (Kumar et al., 2020).

Journal of Cell Science (2023) 136, jcs260060. doi:10.1242/jcs.260060

Fig. 6. The deletion of Yme1 affects the stability of the TIM22 complex. (A) Estimation of steady-state protein levels of the carrier translocase machinery. 100 µg of mitochondria isolated from the indicated strains grown in YPG medium at 37°C were analyzed by SDS-PAGE and western blotting. Protein amounts were quantified using ImageJ software and were plotted as percentages by setting the intensities of WT mitochondria as 100%. Data indicate mean±s.e.m. of *n*=3 biological replicates. Two-way ANOVA with Tukey's multiple-comparisons test was used for calculating statistical significance. n.s., not significant. (B) Assessment of the stability of the carrier translocase machinery using BN-PAGE. Mitochondria isolated from WT, *tim18Δ*, *yme1Δ and tim18Δ yme1Δ* cells grown at 30°C in YPG were solubilized in digitonin buffer, and the proteins were assessed by BN-PAGE followed by immunoblotting with the indicated antibodies. Arrowheads indicate the TIM22 complex (~300 kDa) and the asterisk indicates possible intermediate subcomplexes. The double asterisk denotes the presence of a non-specific band. (C–E) Analysis of the interaction between the carrier translocase machinery and the YME1 complex by co-IP assay. Mitochondria isolated from WT and strains expressing either Tim18–FLAG, Tim23–FLAG or SOD1–FLAG were solubilized in 1% digitonin buffer. The solubilized material was subjected to co-IP assay using anti-FLAG-conjugated protein G Sepharose beads. The bound proteins were examined by immunoblotting using specific antibodies for the indicated proteins; 1% of the total mitochondrial lysate (input) was used as a loading control. The images shown in B–E are representative of *n*=3 experiments.

Media and growth conditions

Yeast cells were grown in YPD (1% yeast extract, 2% peptone and 2% dextrose), YPG (1% yeast extract, 2% peptone and 2% glycerol), SCD–Trp (0.67% yeast nitrogen base without amino acids, 0.069% Trp dropout supplement and 2% dextrose), SCD–Ura (0.67% yeast nitrogen base without amino acids, 0.072% Ura dropout supplement and 2% dextrose), SCD–Ura–Trp (0.67% yeast nitrogen base without amino acids, 0.069% Ura Trp dropout supplement and 2% dextrose) or SCG–Ura (0.67% yeast nitrogen base without amino acids, 0.072% Ura dropout supplement and 3% glycerol) media.

Strains harboring the *kanMX4* or *hphNT1* selection marker were selected on YPD supplemented with either 400 µg ml^{-1} G418 sulfate or 250 µg ml^{-1} hygromycin. Yeast cells were streaked and cultured on SCD containing 1 mg ml^{-1} 5-fluoroorotic acid to remove the *URA3*-harboring plasmid.

Growth phenotype analysis

For spot assay, the respective yeast strains were grown at 30°C in YPD or the indicated media up to the mid-log phase. Cells were harvested by centrifugation (2200 ***g*** for 5 min at room temperature) followed by serial dilution and spotting on YPD, YPG or other required minimal media. The plates were incubated at various temperatures, followed by documentation of images at appropriate time intervals.

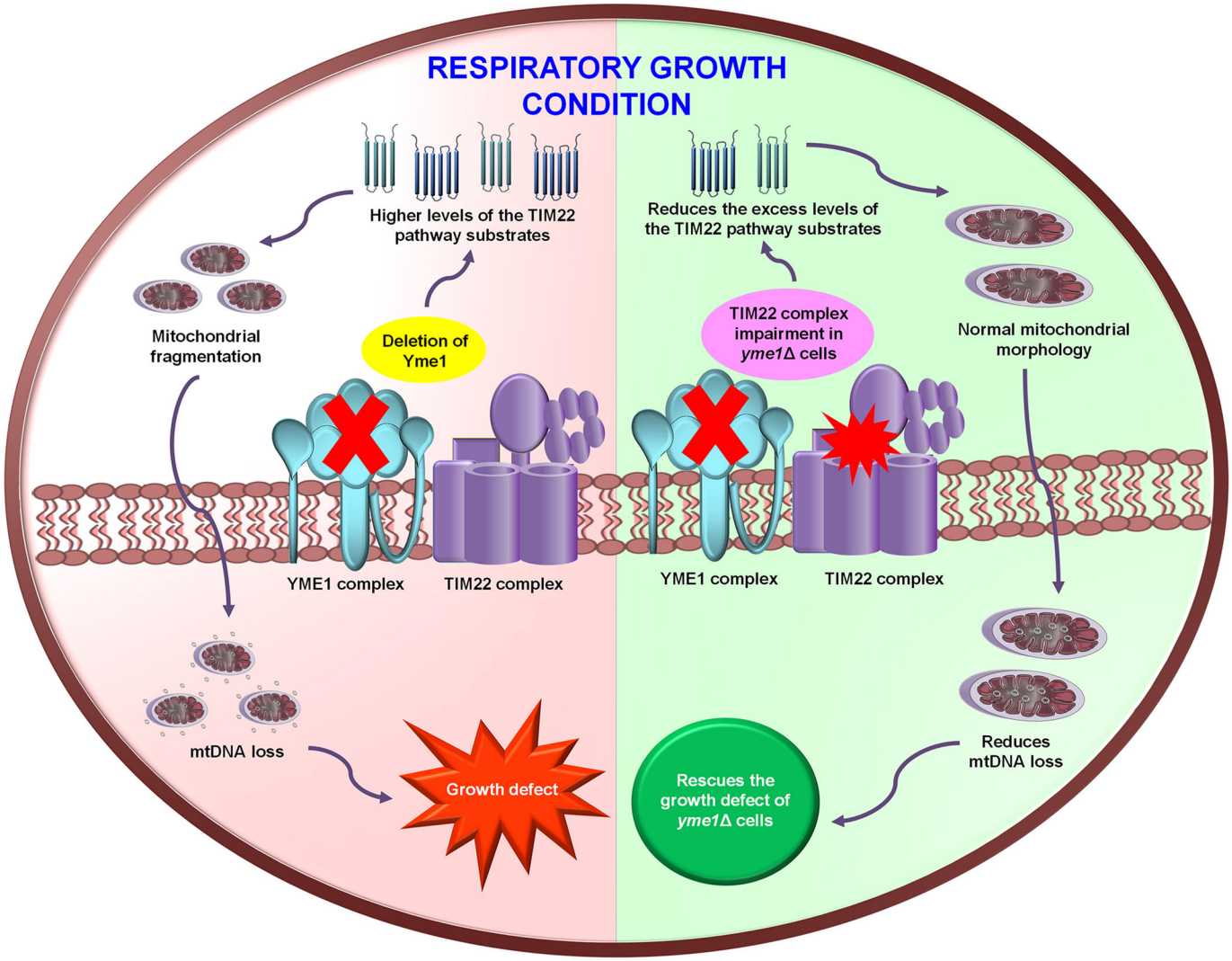

Fig. 7. Diagram highlighting the significance of functional crosstalk between the carrier translocase machinery and the YME1 complex. Under respiratory growth conditions, cells lacking Yme1 exhibit growth defects and mitochondrial fragmentation owing to compromised mitochondrial proteostasis and enhanced mitochondrial DNA (mtDNA) loss. Impairment in the TIM22 complex rescues the growth and mitochondrial defects of cells devoid of Yme1 by decreasing the mitochondrial DNA loss and reducing the excess levels of the TIM22 complex substrates, thereby maintaining mitochondrial quality control.

Journal of Cell Science (2023) 136, jcs260060. doi:10.1242/jcs.260060

For growth curve examination, WT and deletion strains were cultured at 30°C in YPD for 12 h. Following this, an equal amount of cells (absorbance at 600 nm or A_{600}=0.07) were harvested by centrifugation (2200 ***g*** for 5 min at room temperature), washed twice with sterile water and re-inoculated in 50 ml YPG. Absorbance was measured at 600 nm every 12 h intervals for 4 to 5 days using an ultraviolet-visible spectrophotometer (Eppendorf, Hamburg, Germany).

Whole-cell lysate preparation

Total cell protein lysates were prepared by the trichloroacetic acid (TCA; Sigma-Aldrich, T0699-100ML) precipitation method. Equal numbers of cells (A_{600}=5) were harvested by centrifugation at 16,900 ***g*** for 5 min at room temperature, resuspended in 10% TCA, vortexed thoroughly and incubated for 30 min at 4°C with gentle vortexing at 10 min intervals. The samples were centrifuged (2200 ***g*** for 5 min at 4°C) and TCA was removed completely. The resultant pellet was washed twice with acetone, followed by incubation at 42°C for 10 min. Acid-washed 0.5 mm glass beads were added in a 1:1 ratio (w/w) to the pellet along with 1× SDS-PAGE sample buffer (50 mM Tris-HCl, pH 6.8, 2% SDS, 0.1% Bromophenol Blue, 10% glycerol and 100 mM β-mercaptoethanol) and vortexed at maximum speed ten times with intermittent incubation at room temperature. The samples were boiled at 90°C for 10 min, and the final whole-cell lysate was extracted by centrifugation (16,900 ***g*** for 10 min at room temperature). Lysate volumes equivalent to A_{600}=0.5 or 1 (depending on protein abundance) were resolved by SDS-PAGE followed by western blotting.

Evaluation of OCR by Seahorse XF HS mini analyzer

The respiratory capacity was assessed using the Seahorse XF HS mini analyzer (Agilent Technologies, Santa Clara, CA). Seahorse XFp cell culture miniplates were coated with 50 µg ml^{-1} poly-D-lysine (50 µl each well) (Sigma-Aldrich, P6407-5MG) for 30 min at room temperature, and then aspirated followed by air drying at room temperature for 2 h. The Seahorse XFp extracellular flux cartridge was hydrated with sterile water (200 µl per well) and incubated overnight at 37°C in a non-CO_2 incubator and Seahorse XF calibrant solution (Agilent Technologies). After incubation, the water was removed, then the calibrant solution (200 µl per well) was added to the sensor cartridge and incubated at 37°C for 1 h before measurement.

Yeast cultures of WT and the deletion strains were grown in YPD medium at 30°C for 12 h, followed by subculturing in YPG medium at 30°C for 8 h. The cultures were then shifted to 37°C for 8 h to induce the phenotype. For measurement, all cultures were diluted to A_{600}=0.01 to seed cells in wells into a poly-D-lysine-coated Seahorse XFp cell culture miniplate in 50 µl of Seahorse XF assay medium (Agilent Technologies). For background measurement, two wells containing only assay medium were included. The loaded plate was centrifuged at 300 ***g*** for 1 min at room temperature with no brakes. After centrifugation, the volume of the medium was made up to 180 µl, and the loaded plate was incubated for 30 min at 37°C in a non-CO_2 to facilitate the transition of the plate into the temperature of the Seahorse machine. For maximal and non-mitochondrial respiration rates, 4 µM FCCP was added to port A (Seahorse XFp Cell Mito Stress Test Kit, Agilent Technologies, Wilmington, DE) and 1.4 µM rotenone/antimycin A in port B (Agilent Seahorse XFp Cell Mito Stress Test Kit). Four readings were taken for basal respiration, whereas six measurements were recorded after FCCP and rotenone/antimycin A injections.

Imaging mitochondrial morphology and mitochondrial DNA by microscopy

The mitochondrial morphology was analyzed following a prior procedure (Bankapalli et al., 2015). Yeast strains were transformed with the pRS416$_{TEF}$ MTS–mCherry construct (Bankapalli et al., 2015) to visualize the mitochondrial morphology. MTS–mCherry specifically decorates the mitochondria as it contains MTS from subunit 9 of ATP synthase (pSU9), thereby allowing visualization of the mitochondrial network. WT and deletion strains were grown to the mid-log phase in SCG–Ura at 30°C. The cells were then harvested by centrifugation (2200 ***g*** for 5 min at room temperature) followed by final suspension in 1× PBS. The slides were prepared by placing cells (A_{600}=0.1) on 2% agarose pads and covering them with a coverslip. The images were acquired with a Delta Vision Elite fluorescence microscope (GE Healthcare) using a 100× objective lens by keeping a uniform exposure throughout the experiment. The excitation wavelength of 587 nm and the emission wavelength of 610 nm were used for mCherry fluorescence imaging. The images were deconvolved and examined using SoftWoRx 6.1.3 software (GE Healthcare).

For mitochondrial DNA visualization, the corresponding yeast cells were allowed to grow up to the mid-log phase in YPG at 30°C and harvested by centrifugation (2200 ***g*** for 5 min at room temperature). The cells were resuspended in 1× PBS followed by staining with 10 µM SYTO 18 [Yeast Mitochondrial Stain Sampler Kit (Cat. No. Y7530), Thermo Fisher Scientific] for 15 min at 30°C. After this, the cells were thoroughly washed twice with 1× PBS and placed on agarose pads. Images were captured with Delta Vision Elite Fluorescence Microscope (GE Healthcare) using a 100× objective lens. The excitation wavelength of 468 nm and the emission wavelength of 533 nm was used for monitoring SYTO 18 fluorescence. The images were processed using SoftWoRx 6.1.3. software.

Assessment of mitochondrial DNA transfer frequency

The rates of mitochondrial DNA transfer were determined as described previously (Thorsness et al., 1993; Thorsness and Fox, 1993). Yeast strains were grown in YPD and equal numbers of cells (A_{600}=0.5) were harvested by centrifugation (2200 ***g*** for 5 min at room temperature). The cells were resuspended in sterile water, followed by plating on a synthetic growth medium lacking the amino acid tryptophan. The number of colonies obtained was counted to calculate the frequency of mitochondrial DNA transmission.

Measurement of mitochondrial ATP levels

ATP levels were estimated using the ATP detection reagent of the Mitochondrial ToxGlo Assay kit (Promega, Madison, WI). 50 µg mitochondria from WT and deletion strains grown at 30°C in YPG medium were lysed by snap freezing the mitochondria in liquid nitrogen followed by thawing on ice twice. The ATP detection substrate was added in a 1:1 volume to the mitochondrial lysate, and the luminescence was recorded using Glomax Explorer (Promega).

BN-PAGE

BN-PAGE was carried out following a previously published protocol (Wittig et al., 2006). Briefly, mitochondria (2 mg ml^{-1}) were solubilized in 100 µl of digitonin buffer (1% digitonin, 50 mM NaCl, 50 mM imidazole, 2 mM 6-aminohexanoic acid, 1 mM EDTA, pH 7.0) for 30 min at 4°C. The solubilized portion was separated by centrifugation (16,900 ***g*** for 20 min at 4°C), and 15 µl of sample buffer (2.5 µl of 5% Coomassie Brilliant Blue G and 12.5 µl of 50% glycerol) was added per 100 µl of the supernatant fraction. Samples were run on a 6–16% gradient native imidazole PAGE gel, followed by western blotting and immunodetection using antibodies specific to Tim54, Tim22 and porin.

Co-IP

Mitochondria (5 mg ml^{-1}) were solubilized in 1 ml of digitonin buffer [1% digitonin, 25 mM Tris-HCl pH 7.4, 50 mM KCl, 5 mM EDTA, 10% glycerol, 1 mM phenylmethylsulfonyl fluoride (PMSF)]. The insoluble portion was removed by centrifugation (16,900 ***g*** for 20 min at 4°C), and the solubilized fraction was then incubated with 100 µl of protein G Sepharose beads prebound to anti-FLAG antibodies. The samples were allowed to gently rotate at 4°C for 12 h followed by three washes with 1 ml of buffer (0.05% digitonin, 25 mM Tris-HCl, 50 mM KCl, 5 mM EDTA, 10% glycerol, 1 mM PMSF, pH 7.4). The immunoprecipitated proteins were eluted by boiling at 65°C for 10 min in a 1× SDS-PAGE sample buffer. The samples were separated on SDS-PAGE and examined by immunoblotting using specific antibodies for the indicated proteins.

Antibodies and reagents

Antisera specific for Tim22 (1:250), Aac2 (1:250) and Dic1 (1:250) were gifted by Prof. Agnieszka Chacinska (Warsaw University, Poland). Antisera against Sdh3 (1:250) and Yme1 (1:250) were gifted by Prof. Nikolaus Pfanner (University of Freiburg, Germany). Antiserum specific for Tim54

(1:1000) was gifted by Prof. Toshiya Endo (Kyoto Sangyo University, Japan). Antisera against Tim44 (1:5000), Ssb1 (1:3000) and Ssa1 (1:3000) were gifted by Prof. Elizabeth A. Craig. Antiserum specific for PGK1 (1:7000) was gifted by Prof. P. N. Rangarajan (Indian Institute of Science, Bangalore, India). Antibodies against Tim18 (1:2500), Hsp31 (1:3000), Tim23 (1:5000) and Tim50 (1:5000) were raised in rabbits as reported previously (Pareek et al., 2013; Bankapalli et al., 2015; Kumar et al., 2020). The anti-FLAG tag antibody (1:1000) raised in mouse (F1804) and anti-SOD1 antibody (1:3000) raised in rabbit (HPA001401) were obtained from Sigma-Aldrich and the anti-porin antibody (1:5000) raised in mouse (16G9E6BC4) was purchased from Invitrogen.

Yeast extract, peptone, dextrose and agar were purchased from BD Difco. Yeast nitrogen base without amino acids (Y2030-01), 5-fluoroorotic acid (207291-81-4), G418 sulphate (108321-42-2), and zymolyase (37340-57-1) were purchased from US Biological Life Sciences. Hygromycin (CAS 31282-04-9) and digitonin (CAS 11024-24-1) were purchased from Calbiochem. Other fine chemicals or reagents were purchased from Sigma-Aldrich unless specified.

Miscellaneous

Mitochondria were isolated following a previously published protocol (Gambill et al., 1993). Western blotting was performed using standard protocols, and the immunoblots were probed using an enhanced chemiluminescence system from Bio-Rad (1705060). The primers used in this study were manufactured by Sigma-Aldrich, and sequencing reactions were carried out by AgriGenome Labs (India). Uncropped blot images are provided in the Fig. S6.

Statistical analysis

The protein bands were quantified using ImageJ software. Further calculations were performed in Excel (Microsoft), and all statistical analyses were executed using GraphPad Prism 6.0 software. Significance testing was performed using one-way or two-way ANOVA, and Tukey's multiple-comparison test was used to compare different deletion strain values against WT. P-value of <0.05 was considered significant. All indicated n numbers represent biological replicates.

Acknowledgements

We thank Prof. Thomas Fox for providing yeast strains (PTY44 and PTY52); Prof. Toshiya Endo (Kyoto Sangyo University, Japan) for giving yeast strains (WT Tim22-316 and Tim18–FLAG/WT Tim22-316) as well as Tim54 antibodies; Prof. Elizabeth A. Craig (University of Wisconsin-Madison, USA) for antibodies against Tim44, Ssb1 and Ssa1 and yeast vectors (pRS316, pRS414$_{TEF}$ and pRS416$_{TEF}$); Prof. Agnieszka Chacinska (Warsaw University, Poland) for antibodies against Tim22, Aac2, and Dic1; Prof. Nikolaus Pfanner (University of Freiburg, Germany) for antibodies against Sdh3 and Yme1; and Prof. P. N. Rangarajan (Indian Institute of Science, Bangalore, India) for antibodies against PGK1. We acknowledge the central facility of Department of Biochemistry for Seahorse-related experiments. We thank Dr. Sandeep M. Eswarappa for providing Glomax Explorer to analyze luminescence-based experiments. We thank Vinaya Vishwanathan of P.D.'s laboratory for their constructive and critical comments related to the manuscript and microscopy experiments.

Competing interests

The authors declare no competing or financial interests.

Author contributions

Conceptualization: A.K., P.D.; Methodology: A.K.; Validation: A.K., P.D.; Formal analysis: A.K., T.P.W.; Investigation: A.K., T.P.W.; Resources: A.K., P.D.; Writing - original draft: A.K.; Writing - review & editing: A.K., T.P.W., P.D.; Visualization: P.D.; Supervision: P.D.; Project administration: P.D.; Funding acquisition: P.D.

Funding

This work was supported by the Swarnajayanthi Fellowship from the Department of Science and Technology, Ministry of Science and Technology, India (DST/SJF/LS-01/2011–2012), the Department of Biotechnology, Ministry of Science and Technology, India DBT-IISC Partnership Program Phase-II (BT/PR27952/IN/22/212/2018), and the Department of Science and Technology, Ministry of Science and Technology, India DST-FIST Programme-Phase III (SR/FST/LSII-045/2016(G) to P.D. A.K. and T.P.W. acknowledge a research fellowship from the Council of Scientific and Industrial Research, India.

Data availability

All relevant data can be found within the article and its supplementary information.

References

Acoba, M. G., Alpergin, E. S. S., Renuse, S., Fernández-del-Río, L., Lu, Y.-W., Khalimonchuk, O., Clarke, C. F., Pandey, A., Wolfgang, M. J. and Claypool, S. M. (2021). The mitochondrial carrier SFXN1 is critical for complex III integrity and cellular metabolism. *Cell Rep.* **34**, 108869. doi:10.1016/j.celrep.2021.108869

Adam, A., Endres, M., Sirrenberg, C., Lottspeich, F., Neupert, W. and Brunner, M. (1999). Tim9, a new component of the TIM22.54 translocase in mitochondria. *EMBO J.* **18**, 313-319. doi:10.1093/emboj/18.2.313

Araiso, Y., Tsutsumi, A., Qiu, J., Imai, K., Shiota, T., Song, J., Lindau, C., Wenz, L.-S., Sakaue, H., Yunoki, K. et al. (2019). Structure of the mitochondrial import gate reveals distinct preprotein paths. *Nature* **575**, 395-401. doi:10.1038/s41586-019-1680-7

Baker, M. J., Frazier, A. E., Gulbis, J. M. and Ryan, M. T. (2007). Mitochondrial protein-import machinery: correlating structure with function. *Trends Cell Biol.* **17**, 456-464. doi:10.1016/j.tcb.2007.07.010

Bankapalli, K., Saladi, S. D., Awadia, S. S., Goswami, A. V., Samaddar, M. and D'silva, P. (2015). Robust glyoxalase activity of Hsp31, a ThiJ/DJ-1/PfpI family member protein, is critical for oxidative stress resistance in Saccharomyces cerevisiae. *J. Biol. Chem.* **290**, 26491-26507. doi:10.1074/jbc.M115.673624

Bauer, M. F., Rothbauer, U., Mühlenbein, N., Smith, R. J., Gerbitz, K., Neupert, W., Brunner, M. and Hofmann, S. (1999). The mitochondrial TIM22 preprotein translocase is highly conserved throughout the eukaryotic kingdom. *FEBS Lett.* **464**, 41-47. doi:10.1016/S0014-5793(99)01665-8

Callegari, S., Richter, F., Chojnacka, K., Jans, D. C., Lorenzi, I., Pacheu-Grau, D., Jakobs, S., Lenz, C., Urlaub, H., Dudek, J. et al. (2016). TIM29 is a subunit of the human carrier translocase required for protein transport. *FEBS Lett.* **590**, 4147-4158. doi:10.1002/1873-3468.12450

Callegari, S., Müller, T., Schulz, C., Lenz, C., Jans, D. C., Wissel, M., Opazo, F., Rizzoli, S. O., Jakobs, S., Urlaub, H. et al. (2019). A MICOS-TIM22 association promotes carrier import into human mitochondria. *J. Mol. Biol.* **431**, 2835-2851. doi:10.1016/j.jmb.2019.05.015

Campbell, C. L. and Thorsness, P. E. (1998). Escape of mitochondrial DNA to the nucleus in yme1 yeast is mediated by vacuolar-dependent turnover of abnormal mitochondrial compartments. *J. Cell Sci.* **111**, 2455-2464. doi:10.1242/jcs.111.16.2455

Campbell, C. L., Tanaka, N., White, K. H. and Thorsness, P. E. (1994). Mitochondrial morphological and functional defects in yeast caused by yme1 are suppressed by mutation of a 26S protease subunit homologue. *Mol. Biol. Cell* **5**, 899-905. doi:10.1091/mbc.5.8.899

Cesnekova, J., Rodinova, M., Hansikova, H., Zeman, J. and Stiburek, L. (2018). Loss of mitochondrial AAA proteases AFG3L2 and YME1L impairs mitochondrial structure and respiratory chain biogenesis. *Int. J. Mol. Sci.* **19**, 3930. doi:10.3390/ijms19123930

Chacinska, A., Koehler, C. M., Milenkovic, D., Lithgow, T. and Pfanner, N. (2009). Importing mitochondrial proteins: machineries and mechanisms. *Cell* **138**, 628-644. doi:10.1016/j.cell.2009.08.005

Cheng, X. and Ivessa, A. S. (2010). The migration of mitochondrial DNA fragments to the nucleus affects the chronological aging process of Saccharomyces cerevisiae. *Aging Cell* **9**, 919-923. doi:10.1111/j.1474-9726.2010.00607.x

Coyne, L. P. and Chen, X. J. (2018). mPOS is a novel mitochondrial trigger of cell death - implications for neurodegeneration. *FEBS Lett.* **592**, 759-775. doi:10.1002/1873-3468.12894

Coyne, L. P. and Chen, X. J. (2019). Consequences of inner mitochondrial membrane protein misfolding. *Mitochondrion* **49**, 46-55. doi:10.1016/j.mito.2019.06.001

Dudek, J., Rehling, P. and van der Laan, M. (2013). Mitochondrial protein import: common principles and physiological networks. *Biochim. Biophys. Acta* **1833**, 274-285. doi:10.1016/j.bbamcr.2012.05.028

Dukanovic, J. and Rapaport, D. (2011). Multiple pathways in the integration of proteins into the mitochondrial outer membrane. *Biochim. Biophys. Acta* **1808**, 971-980. doi:10.1016/j.bbamem.2010.06.021

Dunn, C. D. and Jensen, R. E. (2003). Suppression of a defect in mitochondrial protein import identifies cytosolic proteins required for viability of yeast cells lacking mitochondrial DNA. *Genetics* **165**, 35-45. doi:10.1093/genetics/165.1.35

Dunn, C. D., Tamura, Y., Sesaki, H. and Jensen, R. E. (2008). Mgr3p and Mgr1p are adaptors for the mitochondrial i-AAA protease complex. *Mol. Biol. Cell* **19**, 5387-5397. doi:10.1091/mbc.e08-01-0103

Ellenrieder, L., Dieterle, M. P., Doan, K. N., Martensson, C. U., Floerchinger, A., Campo, M. L., Pfanner, N. and Becker, T. (2019). Dual role of mitochondrial porin in metabolite transport across the outer membrane and protein transfer to the inner membrane. *Mol. Cell* **73**, 1056-1065.e7. doi:10.1016/j.molcel.2018.12.014

Endo, T. and Yamano, K. (2009). Multiple pathways for mitochondrial protein traffic. *Biol. Chem.* **390**, 723-730. doi:10.1515/BC.2009.087

Endres, M., Neupert, W. and Brunner, M. (1999). Transport of the ADP/ATP carrier of mitochondria from the TOM complex to the TIM22.54 complex. *EMBO J.* **18**, 3214-3221. doi:10.1093/emboj/18.12.3214

Gambill, B. D., Voos, W., Kang, P. J., Miao, B., Langer, T., Craig, E. A. and Pfanner, N. (1993). A dual role for mitochondrial heat shock protein 70 in membrane translocation of preproteins. *J. Cell Biol.* **123**, 109-117. doi:10.1083/jcb.123.1.109

Gebert, N., Gebert, M., Oeljeklaus, S., von der Malsburg, K., Stroud, D. A., Kulawiak, B., Wirth, C., Zahedi, R. P., Dolezal, P., Wiese, S. et al. (2011). Dual function of Sdh3 in the respiratory chain and TIM22 protein translocase of the mitochondrial inner membrane. *Mol. Cell* **44**, 811-818. doi:10.1016/j.molcel.2011.09.025

Gerdes, F., Tatsuta, T. and Langer, T. (2012). Mitochondrial AAA proteases–towards a molecular understanding of membrane-bound proteolytic machines. *Biochim. Biophys. Acta* **1823**, 49-55. doi:10.1016/j.bbamcr.2011.09.015

Gomkale, R., Cruz-Zaragoza, L. D., Suppanz, I., Guiard, B., Montoya, J., Callegari, S., Pacheu-Grau, D., Warscheid, B. and Rehling, P. (2020). Defining the substrate spectrum of the TIM22 complex identifies pyruvate carrier subunits as unconventional cargos. *Curr. Biol.* **30**, 1119-1127.e5. doi:10.1016/j.cub.2020.01.024

Griparic, L., Kanazawa, T. and van der Bliek, A. M. (2007). Regulation of the mitochondrial dynamin-like protein Opa1 by proteolytic cleavage. *J. Cell Biol.* **178**, 757-764. doi:10.1083/jcb.200704112

Hartmann, B., Wai, T., Hu, H., Macvicar, T., Musante, L., Fischer-Zirnsak, B., Stenzel, W., Graf, R., van den Heuvel, L., Ropers, H. H. et al. (2016). Homozygous YME1L1 mutation causes mitochondriopathy with optic atrophy and mitochondrial network fragmentation. *eLife* **5**, e16078. doi:10.7554/eLife.16078

Hines, J. K., Li, X., Du, Z., Higurashi, T., Li, L. and Craig, E. A. (2011). [SWI], the prion formed by the chromatin remodeling factor Swi1, is highly sensitive to alterations in Hsp70 chaperone system activity. *PLoS Genet.* **7**, e1001309. doi:10.1371/journal.pgen.1001309

Horten, P., Colina-Tenorio, L. and Rampelt, H. (2020). Biogenesis of mitochondrial metabolite carriers. *Biomolecules* **10**, 1008. doi:10.3390/biom10071008

Hwang, D. K., Claypool, S. M., Leuenberger, D., Tienson, H. L. and Koehler, C. M. (2007). Tim54p connects inner membrane assembly and proteolytic pathways in the mitochondrion. *J. Cell Biol.* **178**, 1161-1175. doi:10.1083/jcb.200706195

Jackson, T. D., Hock, D. H., Fujihara, K. M., Palmer, C. S., Frazier, A. E., Low, Y. C., Kang, Y., Ang, C. S., Clemons, N. J., Thorburn, D. R. et al. (2021). The TIM22 complex mediates the import of sideroflexins and is required for efficient mitochondrial one-carbon metabolism. *Mol. Biol. Cell* **32**, 475-491. doi:10.1091/mbc.E20-06-0390

Jarosch, E., Tuller, G., Daum, G., Waldherr, M., Voskova, A. and Schweyen, R. J. (1996). Mrs5p, an essential protein of the mitochondrial intermembrane space, affects protein import into yeast mitochondria. *J. Biol. Chem.* **271**, 17219-17225. doi:10.1074/jbc.271.29.17219

Jarosch, E., Rödel, G. and Schweyen, R. J. (1997). A soluble 12-kDa protein of the mitochondrial intermembrane space, Mrs11p, is essential for mitochondrial biogenesis and viability of yeast cells. *Mol. Gen. Genet.* **255**, 157-165. doi:10.1007/s004380050484

Kang, Y., Baker, M. J., Liem, M., Louber, J., McKenzie, M., Atukorala, I., Ang, C.-S., Keerthikumar, S., Mathivanan, S. and Stojanovski, D. (2016). Tim29 is a novel subunit of the human TIM22 translocase and is involved in complex assembly and stability. *eLife* **5**, e17463. doi:10.7554/eLife.17463

Kang, Y., Stroud, D. A., Baker, M. J., De Souza, D. P., Frazier, A. E., Liem, M., Tull, D., Mathivanan, S., McConville, M. J., Thorburn, D. R. et al. (2017). Sengers syndrome-associated mitochondrial acylglycerol kinase is a subunit of the human TIM22 protein import complex. *Mol. Cell* **67**, 457-470.e5. doi:10.1016/j.molcel.2017.06.014

Kang, Y., Fielden, L. F. and Stojanovski, D. (2018). Mitochondrial protein transport in health and disease. *Semin. Cell Dev. Biol.* **76**, 142-153. doi:10.1016/j.semcdb.2017.07.028

Kerscher, O., Holder, J., Srinivasan, M., Leung, R. S. and Jensen, R. E. (1997). The Tim54p-Tim22p complex mediates insertion of proteins into the mitochondrial inner membrane. *J. Cell Biol.* **139**, 1663-1675. doi:10.1083/jcb.139.7.1663

Kerscher, O., Sepuri, N. B. and Jensen, R. E. (2000). Tim18p is a new component of the Tim54p-Tim22p translocon in the mitochondrial inner membrane. *Mol. Biol. Cell* **11**, 103-116. doi:10.1091/mbc.11.1.103

Koehler, C. M., Leuenberger, D., Merchant, S., Renold, A., Junne, T. and Schatz, G. (1999). Human deafness dystonia syndrome is a mitochondrial disease. *Proc. Natl. Acad. Sci. USA* **96**, 2141-2146. doi:10.1073/pnas.96.5.2141

Koehler, C. M., Murphy, M. P., Bally, N. A., Leuenberger, D., Oppliger, W., Dolfini, L., Junne, T., Schatz, G. and Or, E. (2000). Tim18p, a new subunit of the TIM22 complex that mediates insertion of imported proteins into the yeast mitochondrial inner membrane. *Mol. Cell. Biol.* **20**, 1187-1193. doi:10.1128/MCB.20.4.1187-1193.2000

Koppen, M. and Langer, T. (2007). Protein degradation within mitochondria: versatile activities of AAA proteases and other peptidases. *Crit. Rev. Biochem. Mol. Biol.* **42**, 221-242. doi:10.1080/10409230701380452

Kovermann, P., Truscott, K. N., Guiard, B., Rehling, P., Sepuri, N. B., Müller, H., Jensen, R. E., Wagner, R. and Pfanner, N. (2002). Tim22, the essential core of the mitochondrial protein insertion complex, forms a voltage-activated and signal-gated channel. *Mol. Cell* **9**, 363-373. doi:10.1016/S1097-2765(02)00446-X

Kumar, A., Matta, S. K. and D'silva, P. (2020). Conserved regions of budding yeast Tim22 have a role in structural organization of the carrier translocase. *J. Cell Sci.* **133**, jcs244632. doi:10.1242/jcs.244632

Kumar, A., Matta, S. K., Renganathan, V. and D'silva, P. (2022). A journey through the gateway of polytopic inner membrane proteins: the carrier translocase machinery. *Curr. Opin. Physiol.* **26**, 100533. doi:10.1016/j.cophys.2022.100533

Leonhard, K., Stiegler, A., Neupert, W. and Langer, T. (1999). Chaperone-like activity of the AAA domain of the yeast Yme1 AAA protease. *Nature* **398**, 348-351. doi:10.1038/18704

Leonhard, K., Guiard, B., Pellecchia, G., Tzagoloff, A., Neupert, W. and Langer, T. (2000). Membrane protein degradation by AAA proteases in mitochondria: extraction of substrates from either membrane surface. *Mol. Cell* **5**, 629-638. doi:10.1016/S1097-2765(00)80242-7

Leuenberger, D., Bally, N. A., Schatz, G. and Koehler, C. M. (1999). Different import pathways through the mitochondrial intermembrane space for inner membrane proteins. *EMBO J.* **18**, 4816-4822. doi:10.1093/emboj/18.17.4816

Lill, R. and Mühlenhoff, U. (2005). Iron-sulfur-protein biogenesis in eukaryotes. *Trends Biochem. Sci.* **30**, 133-141. doi:10.1016/j.tibs.2005.01.006

Lin, M. T. and Beal, M. F. (2006). Mitochondrial dysfunction and oxidative stress in neurodegenerative diseases. *Nature* **443**, 787-795. doi:10.1038/nature05292

Liu, Y., Wang, X. and Chen, X. J. (2015). Misfolding of mutant adenine nucleotide translocase in yeast supports a novel mechanism of Ant1-induced muscle diseases. *Mol. Biol. Cell* **26**, 1985-1994. doi:10.1091/mbc.E15-01-0030

Liu, Y., Wang, X., Coyne, L. P., Yang, Y., Qi, Y., Middleton, F. A. and Chen, X. J. (2019). Mitochondrial carrier protein overloading and misfolding induce aggresomes and proteostatic adaptations in the cytosol. *Mol. Biol. Cell* **30**, 1272-1284. doi:10.1091/mbc.E19-01-0046

Matta, S. K., Kumar, A. and D'Silva, P. (2020). Mgr2 regulates mitochondrial preprotein import by associating with channel-forming Tim23 subunit. *Mol. Biol. Cell* **31**, 1112-1123. doi:10.1091/mbc.E19-12-0677

Mühlenbein, N., Hofmann, S., Rothbauer, U. and Bauer, M. F. (2004). Organization and function of the small Tim complexes acting along the import pathway of metabolite carriers into mammalian mitochondria. *J. Biol. Chem.* **279**, 13540-13546. doi:10.1074/jbc.M312485200

Neupert, W. and Herrmann, J. M. (2007). Translocation of proteins into mitochondria. *Annu. Rev. Biochem.* **76**, 723-749. doi:10.1146/annurev.biochem.76.052705.163409

Nunnari, J. and Suomalainen, A. (2012). Mitochondria: in sickness and in health. *Cell* **148**, 1145-1159. doi:10.1016/j.cell.2012.02.035

Okamoto, H., Miyagawa, A., Shiota, T., Tamura, Y. and Endo, T. (2004). Intramolecular disulfide bond of Tim22 protein maintains integrity of the TIM22 complex in the mitochondrial inner membrane. *J. Biol. Chem.* **289**, 4827-4838. doi:10.1074/jbc.M113.543264

Pacheu-Grau, D., Callegari, S., Emperador, S., Thompson, K., Aich, A., Topol, S. E., Spencer, E. G., McFarland, R., Ruiz-Pesini, E., Torkamani, A. et al. (2018). Mutations of the mitochondrial carrier translocase channel subunit TIM22 cause early-onset mitochondrial myopathy. *Hum. Mol. Genet.* **27**, 4135-4144. doi:10.1093/hmg/ddy305

Pareek, G., Krishnamoorthy, V. and D'silva, P. (2013). Molecular insights revealing interaction of Tim23 and channel subunits of presequence translocase. *Mol. Cell. Biol.* **33**, 4641-4659. doi:10.1128/MCB.00876-13

Paschen, S. A., Rothbauer, U., Kaldi, K., Bauer, M. F., Neupert, W. and Brunner, M. (2000). The role of the TIM8-13 complex in the import of Tim23 into mitochondria. *EMBO J.* **19**, 6392-6400. doi:10.1093/emboj/19.23.6392

Puchades, C., Rampello, A. J., Shin, M., Giuliano, C. J., Wiseman, R. L., Glynn, S. E. and Lander, G. C. (2017). Structure of the mitochondrial inner membrane AAA+ protease YME1 gives insight into substrate processing. *Science* **358**, eaao0464. doi:10.1126/science.aao0464

Qi, L., Wang, Q., Guan, Z., Wu, Y., Shen, C., Hong, S., Cao, J., Zhang, X., Yan, C. and Yin, P. (2021). Cryo-EM structure of the human mitochondrial translocase TIM22 complex. *Cell Res.* **31**, 369-372. doi:10.1038/s41422-020-00400-w

Rainbolt, T. K., Atanassova, N., Genereux, J. C. and Wiseman, R. L. (2013). Stress-regulated translational attenuation adapts mitochondrial protein import through Tim17A degradation. *Cell Metab.* **18**, 908-919. doi:10.1016/j.cmet.2013.11.006

Rampelt, H., Sucec, I., Bersch, B., Horten, P., Perschil, I., Martinou, J.-C., van der Laan, M., Wiedemann, N., Schanda, P. and Pfanner, N. (2020). The mitochondrial carrier pathway transports non-canonical substrates with an odd number of transmembrane segments. *BMC Biol.* **18**, 2. doi:10.1186/s12915-019-0733-6

Rehling, P., Model, K., Brandner, K., Kovermann, P., Sickmann, A., Meyer, H. E., Kuhlbrandt, W., Wagner, R., Truscott, K. N. and Pfanner, N. (2003). Protein insertion into the mitochondrial inner membrane by a twin-pore translocase. *Science* **299**, 1747-1751. doi:10.1126/science.1080945

Rehling, P., Brandner, K. and Pfanner, N. (2004). Mitochondrial import and the twin-pore translocase. *Nat. Rev. Mol. Cell Biol.* **5**, 519-530. doi:10.1038/nrm1426

Roesch, K., Curran, S. P., Tranebjaerg, L. and Koehler, C. M. (2002). Human deafness dystonia syndrome is caused by a defect in assembly of the DDP1/

TIMM8a-TIMM13 complex. *Hum. Mol. Genet.* **11**, 477-486. doi:10.1093/hmg/11.5.477

Ruan, L., Wang, Y., Zhang, X., Tomaszewski, A., Mcnamara, J. T. and Li, R. (2020). Mitochondria-associated proteostasis. *Annu. Rev. Biophys.* **49**, 41-67. doi:10.1146/annurev-biophys-121219-081604

Schendzielorz, A. B., Bragoszewski, P., Naumenko, N., Gomkale, R., Schulz, C., Guiard, B., Chacinska, A. and Rehling, P. (2018). Motor recruitment to the TIM23 channel's lateral gate restricts polypeptide release into the inner membrane. *Nat. Commun.* **9**, 4028. doi:10.1038/s41467-018-06492-8

Schmidt, O., Pfanner, N. and Meisinger, C. (2010). Mitochondrial protein import: from proteomics to functional mechanisms. *Nat. Rev. Mol. Cell Biol.* **11**, 655-667. doi:10.1038/nrm2959

Sirrenberg, C., Bauer, M. F., Guiard, B., Neupert, W. and Brunner, M. (1996). Import of carrier proteins into the mitochondrial inner membrane mediated by Tim22. *Nature* **384**, 582-585. doi:10.1038/384582a0

Song, J., Herrmann, J. M. and Becker, T. (2021). Quality control of the mitochondrial proteome. *Nat. Rev. Mol. Cell Biol.* **22**, 54-70. doi:10.1038/s41580-020-00300-2

Spiller, M. P., Guo, L., Wang, Q., Tran, P. and Lu, H. (2015). Mitochondrial Tim9 protects Tim10 from degradation by the protease Yme1. *Biosci. Rep.* **35**, e00193. doi:10.1042/BSR20150038

Stiburek, L., Cesnekova, J., Kostkova, O., Fornuskova, D., Vinsova, K., Wenchich, L., Houstek, J. and Zeman, J. (2012). YME1L controls the accumulation of respiratory chain subunits and is required for apoptotic resistance, cristae morphogenesis, and cell proliferation. *Mol. Biol. Cell* **23**, 1010-1023. doi:10.1091/mbc.e11-08-0674

Stojanovski, D., Bragoszewski, P. and Chacinska, A. (2012). The MIA pathway: a tight bond between protein transport and oxidative folding in mitochondria. *Biochim. Biophys. Acta* **1823**, 1142-1150. doi:10.1016/j.bbamcr.2012.04.014

Tatsuta, T. and Langer, T. (2008). Quality control of mitochondria: protection against neurodegeneration and ageing. *EMBO J.* **27**, 306-314. doi:10.1038/sj.emboj.7601972

Thorsness, P. E. and Fox, T. D. (1993). Nuclear mutations in Saccharomyces cerevisiae that affect the escape of DNA from mitochondria to the nucleus. *Genetics* **134**, 21-28. doi:10.1093/genetics/134.1.21

Thorsness, P. E., White, K. H. and Fox, T. D. (1993). Inactivation of YME1, a member of the ftsH-SEC18-PAS1-CDC48 family of putative ATPase-encoding genes, causes increased escape of DNA from mitochondria in Saccharomyces cerevisiae. *Mol. Cell. Biol.* **13**, 5418-5426. doi:10.1128/MCB.13.9.5418

Tilokani, L., Nagashima, S., Paupe, V. and Prudent, J. (2018). Mitochondrial dynamics: overview of molecular mechanisms. *Essays Biochem.* **62**, 341-360. doi:10.1042/EBC20170104

van der Laan, M., Hutu, D. P. and Rehling, P. (2010). On the mechanism of preprotein import by the mitochondrial presequence translocase. *Biochim. Biophys. Acta* **1803**, 732-739. doi:10.1016/j.bbamcr.2010.01.013

Vukotic, M., Nolte, H., König, T., Saita, S., Ananjew, M., Krüger, M., Tatsuta, T. and Langer, T. (2017). Acylglycerol kinase mutated in sengers syndrome is a subunit of the TIM22 protein translocase in mitochondria. *Mol. Cell* **67**, 471-483.e7. doi:10.1016/j.molcel.2017.06.013

Wagner, K., Gebert, N., Guiard, B., Brandner, K., Truscott, K. N., Wiedemann, N., Pfanner, N. and Rehling, P. (2008). The assembly pathway of the mitochondrial carrier translocase involves four preprotein translocases. *Mol. Cell. Biol.* **28**, 4251-4260. doi:10.1128/MCB.02216-07

Wang, X. and Chen, X. J. (2015). A cytosolic network suppressing mitochondria-mediated proteostatic stress and cell death. *Nature* **524**, 481-484. doi:10.1038/nature14859

Wang, X., Zuo, X., Kucejova, B. and Chen, X. J. (2008). Reduced cytosolic protein synthesis suppresses mitochondrial degeneration. *Nat. Cell Biol.* **10**, 1090-1097. doi:10.1038/ncb1769

Wang, K., Jin, M., Liu, X. and Klionsky, D. J. (2013). Proteolytic processing of Atg32 by the mitochondrial i-AAA protease Yme1 regulates mitophagy. *Autophagy* **9**, 1828-1836. doi:10.4161/auto.26281

Weber, E. R., Rooks, R. S., Shafer, K. S., Chase, J. W. and Thorsness, P. E. (1995). Mutations in the mitochondrial ATP synthase gamma subunit suppress a slow-growth phenotype of yme1 yeast lacking mitochondrial DNA. *Genetics* **140**, 435-442. doi:10.1093/genetics/140.2.435

Weber, E. R., Hanekamp, T. and Thorsness, P. E. (1996). Biochemical and functional analysis of the YME1 gene product, an ATP and zinc-dependent mitochondrial protease from S. cerevisiae. *Mol. Biol. Cell* **7**, 307-317. doi:10.1091/mbc.7.2.307

Weidberg, H. and Amon, A. (2018). MitoCPR-A surveillance pathway that protects mitochondria in response to protein import stress. *Science* **360**, eaan4146. doi:10.1126/science.aan4146

Weinhäupl, K., Wang, Y., Hessel, A., Brennich, M., Lindorff-Larsen, K. and Schanda, P. (2021). Architecture and assembly dynamics of the essential mitochondrial chaperone complex TIM9.10.12. *Structure* **29**, 1065-1073.e4. doi:10.1016/j.str.2021.04.009

Wiedemann, N. and Pfanner, N. (2017). Mitochondrial Machineries for Protein Import and Assembly. *Annu. Rev. Biochem.* **86**, 685-714. doi:10.1146/annurev-biochem-060815-014352

Wiedemann, N., van der Laan, M., Hutu, D. P., Rehling, P. and Pfanner, N. (2007). Sorting switch of mitochondrial presequence translocase involves coupling of motor module to respiratory chain. *J. Cell Biol.* **179**, 1115-1122. doi:10.1083/jcb.200709087

Wittig, I., Braun, H.-P. and Schägger, H. (2006). Blue native PAGE. *Nat. Protoc.* **1**, 418-428. doi:10.1038/nprot.2006.62

Wrobel, L., Topf, U., Bragoszewski, P., Wiese, S., Sztolsztener, M. E., Oeljeklaus, S., Varabyova, A., Lirski, M., Chroscicki, P., Mroczek, S. et al. (2015). Mistargeted mitochondrial proteins activate a proteostatic response in the cytosol. *Nature* **524**, 485-488. doi:10.1038/nature14951

Wu, X., Li, L. and Jiang, H. (2018). Mitochondrial inner-membrane protease Yme1 degrades outer-membrane proteins Tom22 and Om45. *J. Cell Biol.* **217**, 139-149. doi:10.1083/jcb.201702125

Zhang, Y., Ou, X., Wang, X., Sun, D., Zhou, X., Wu, X., Li, Q. and Li, L. (2021). Structure of the mitochondrial TIM22 complex from yeast. *Cell Res.* **31**, 366-368. doi:10.1038/s41422-020-00399-0

Zhu, L., Zhou, Q., He, L. and Chen, L. (2021). Mitochondrial unfolded protein response: An emerging pathway in human diseases. *Free Radic. Biol. Med.* **163**, 125-134. doi:10.1016/j.freeradbiomed.2020.12.013

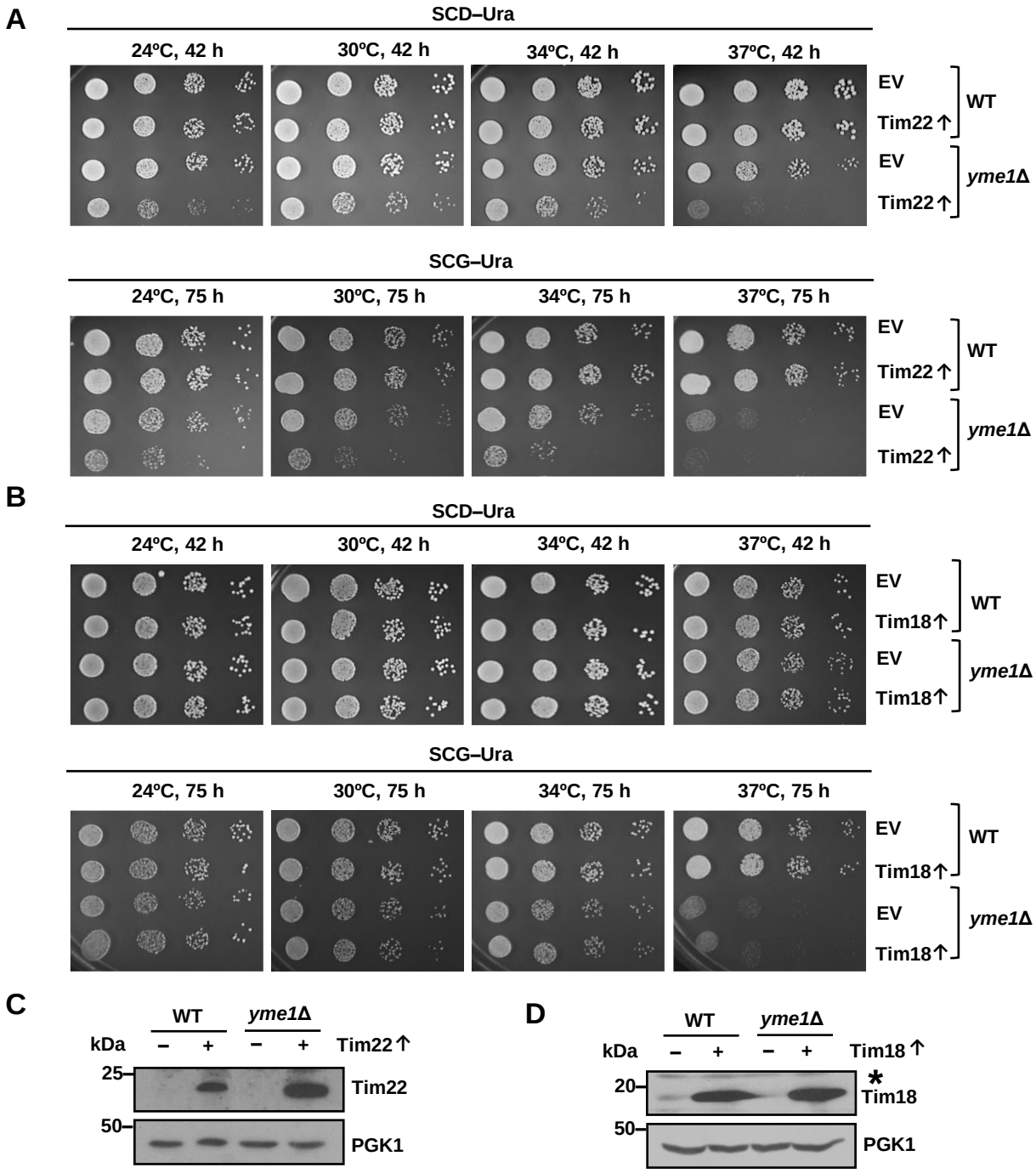

Fig. S1. The overexpression of Tim22 aggravates the growth defects of the *yme1*Δ strain. (A,B) Growth phenotype analysis upon overexpression. WT and *yme1*Δ strains overexpressing either Tim22 or Tim18 under the control of centromeric plasmid pRS416$_{TEF}$ were serially diluted and spotted on the indicated media. (C,D) Examination of steady-state levels of overexpressed proteins. The overexpression of Tim22 and Tim18 were examined by immunoblotting in the whole-cell extracts of the indicated strains. The asterisk indicates the presence of a non-specific band. Data in A–D are representative of *n*=3 experiments.

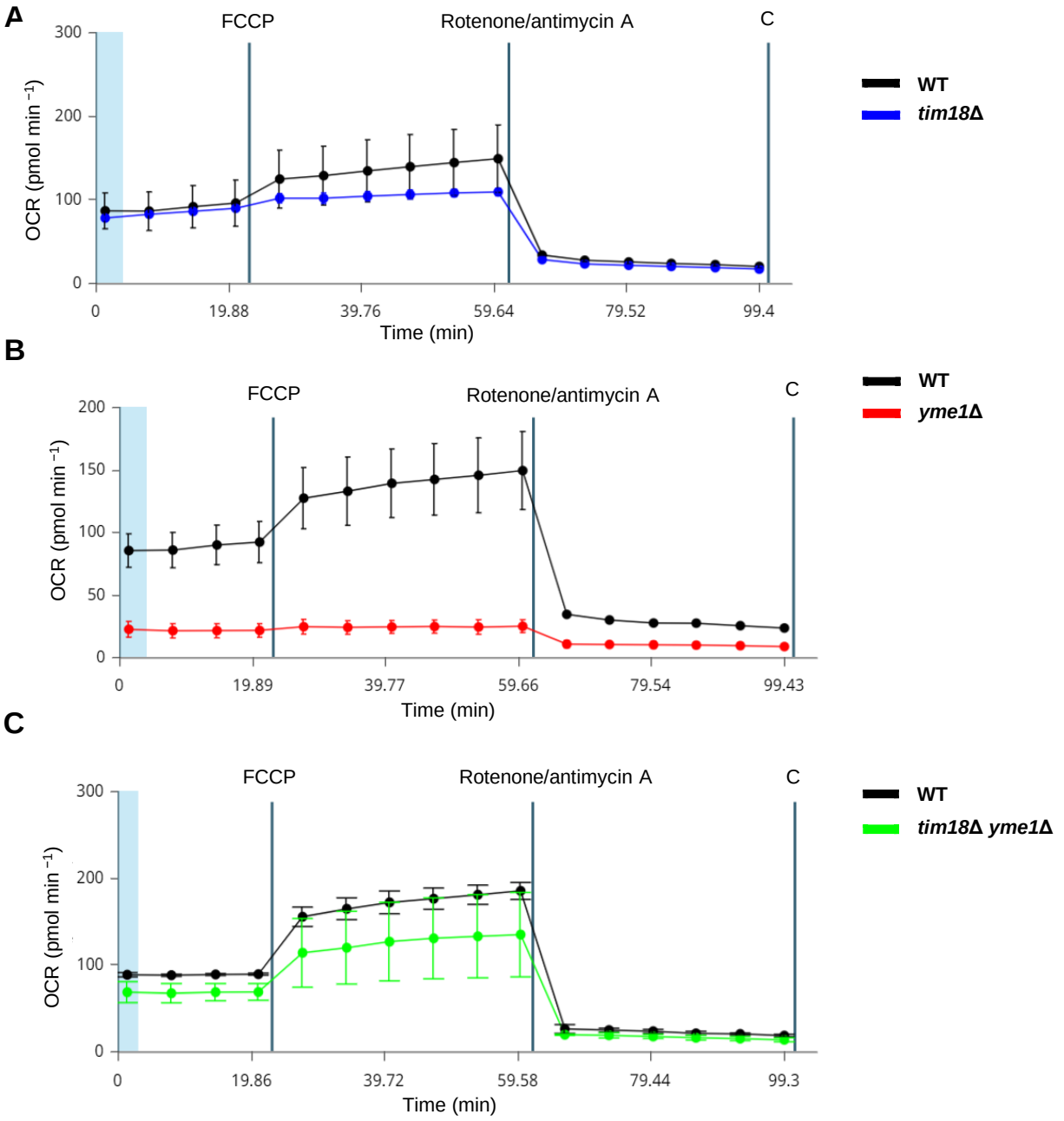

Fig. S2. The deletion of Tim18 rescues the OCR of cells lacking Yme1. (A-C) Measurement of OCRs. The respiratory capacity of WT and the indicated deletion strains were determined with a Seahorse XF HS mini analyzer. FCCP and rotenone/antimycin A were sequentially added to analyze mitochondrial respiratory efficiency. Each graph represents an individual experiment showing the pattern of OCRs for WT and the deletion strains.

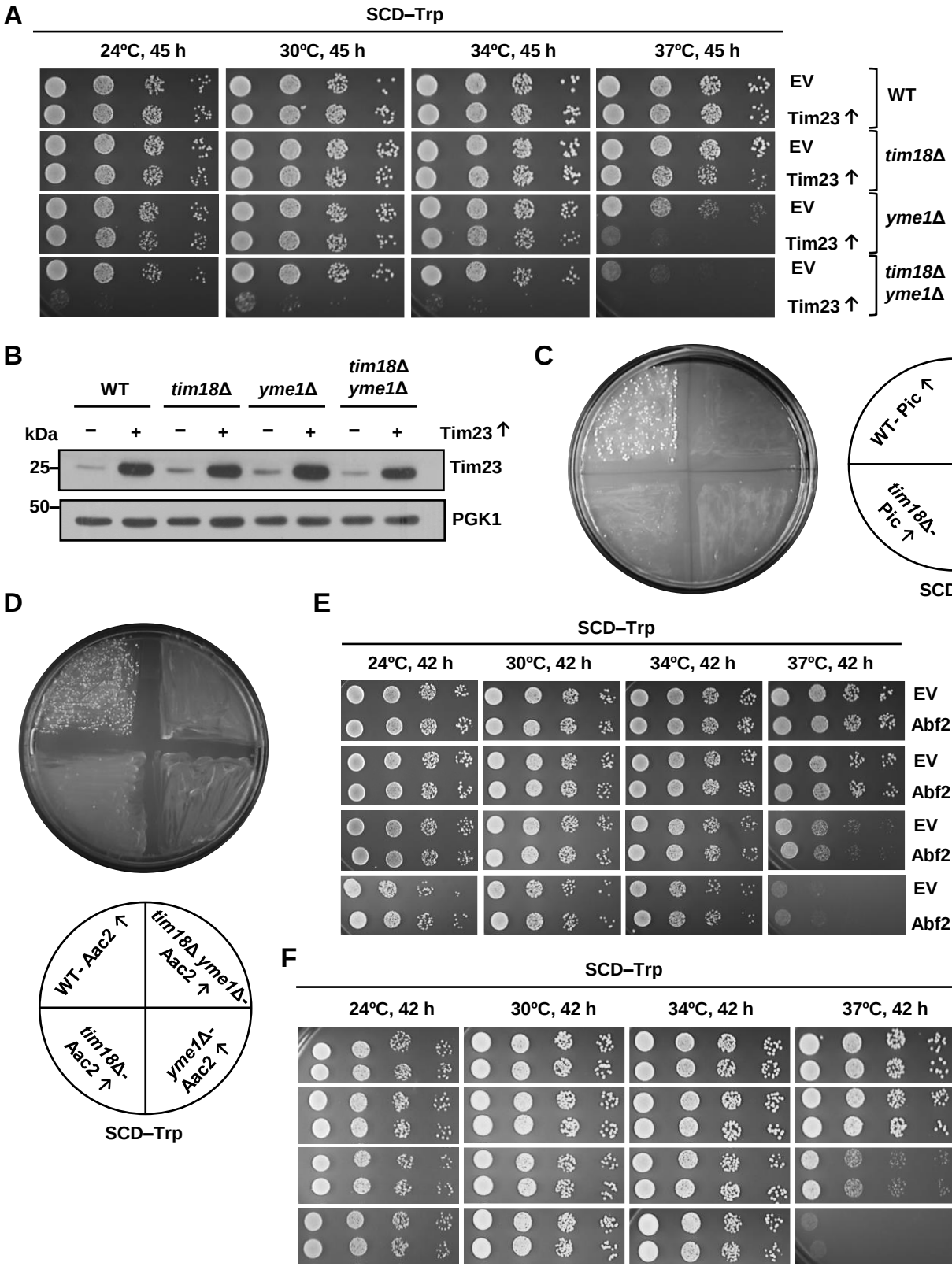

Fig. S3. The overexpression of the TIM22 pathway substrates escalates the growth defects of the *yme1*Δ cells. (A) Growth phenotype analysis upon overexpression of Tim23. Ten-fold serially diluted WT and deletion strains overexpressing Tim23 under the control of centromeric plasmid $pRS414_{TEF}$ were spotted on the SCD–Trp medium and incubated at different temperatures. (B) Estimation of the Tim23 overexpression. The overexpression of Tim23 was examined in the whole-cell extracts of the indicated strains by immunoblotting. (C,D) Assessment of Pic and Aac2 overexpression on the growth of WT and deletion strains. The ORFs of Pic and Aac2 were cloned in the $pRS414_{TEF}$ plasmid and transformed in WT and deletion strains, followed by plating on selection medium (SCD–Trp). (E,F) Examination of growth phenotype upon overexpression of Abf2 and Tom6. WT and deletion strains encompassing either EV, Abf2, or Tom6 overexpressing plasmids were grown to the mid-log phase, serially diluted, and spotted on the specified medium. The images shown are representative of *n*=3 biological replicates.

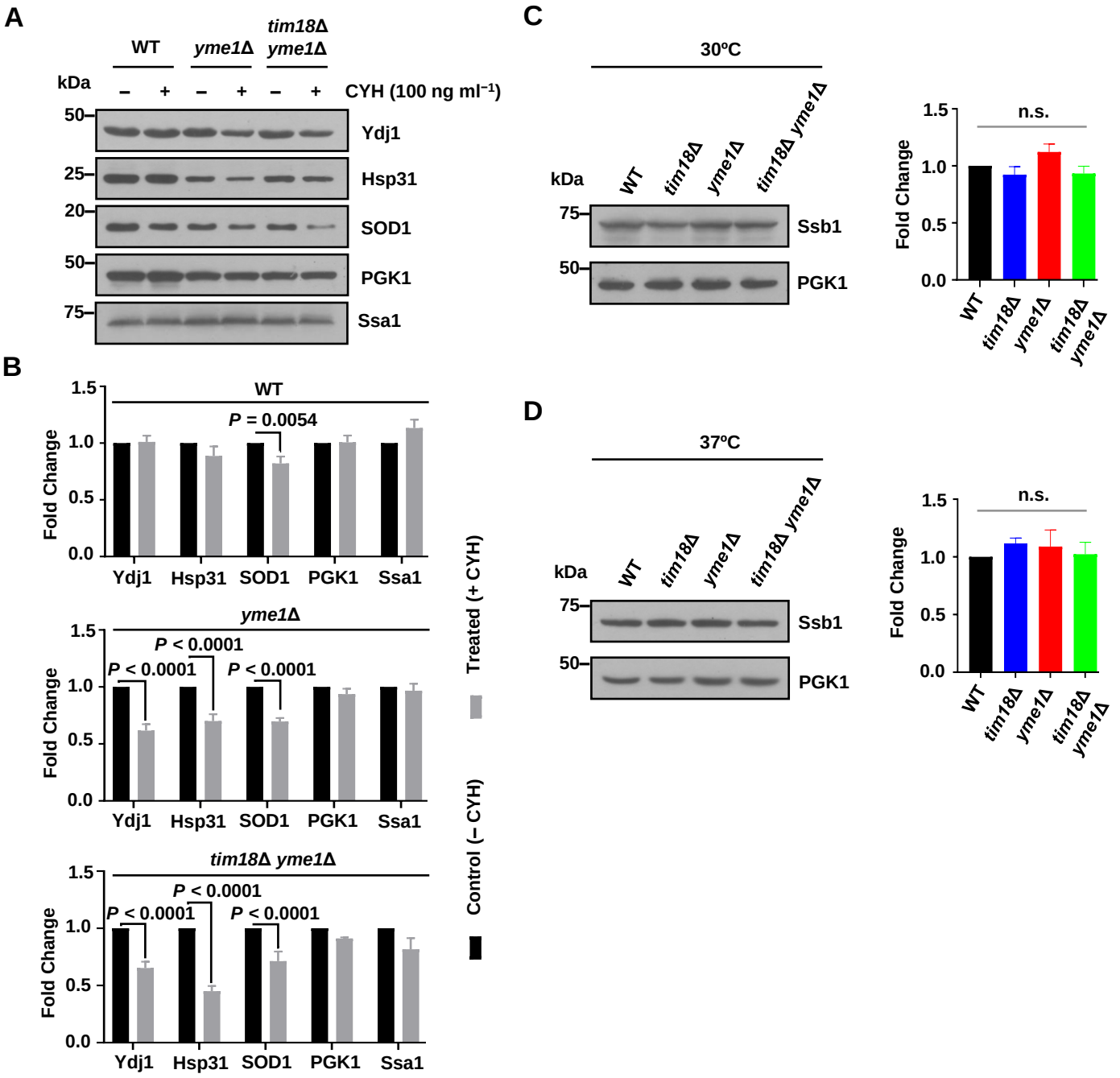

Fig. S4. Partial suppression of cytosolic protein synthesis does not rescue the growth defects of *yme1*Δ cells. (A,B) Assessment of the cytosolic protein inhibition upon CYH treatment. WT, *yme1*Δ, and *tim18*Δ*yme1*Δ strains were treated with CYH (100 ng ml^{-1}) for 180 min, followed by immunoblot analysis of different cytosolic proteins in whole-cell extracts. (C,D) Estimation of Ssb1 steady-state protein levels. The expression of Ssb1 in the whole-cell extracts of WT and the indicated deletion strains was measured by immunoblotting at permissive and elevated temperatures. Data represent mean±s.e.m. of n=3 biological replicates. One-way ANOVA with Tukey's multiple comparisons test was used for determining statistical significance. n.s., not significant.

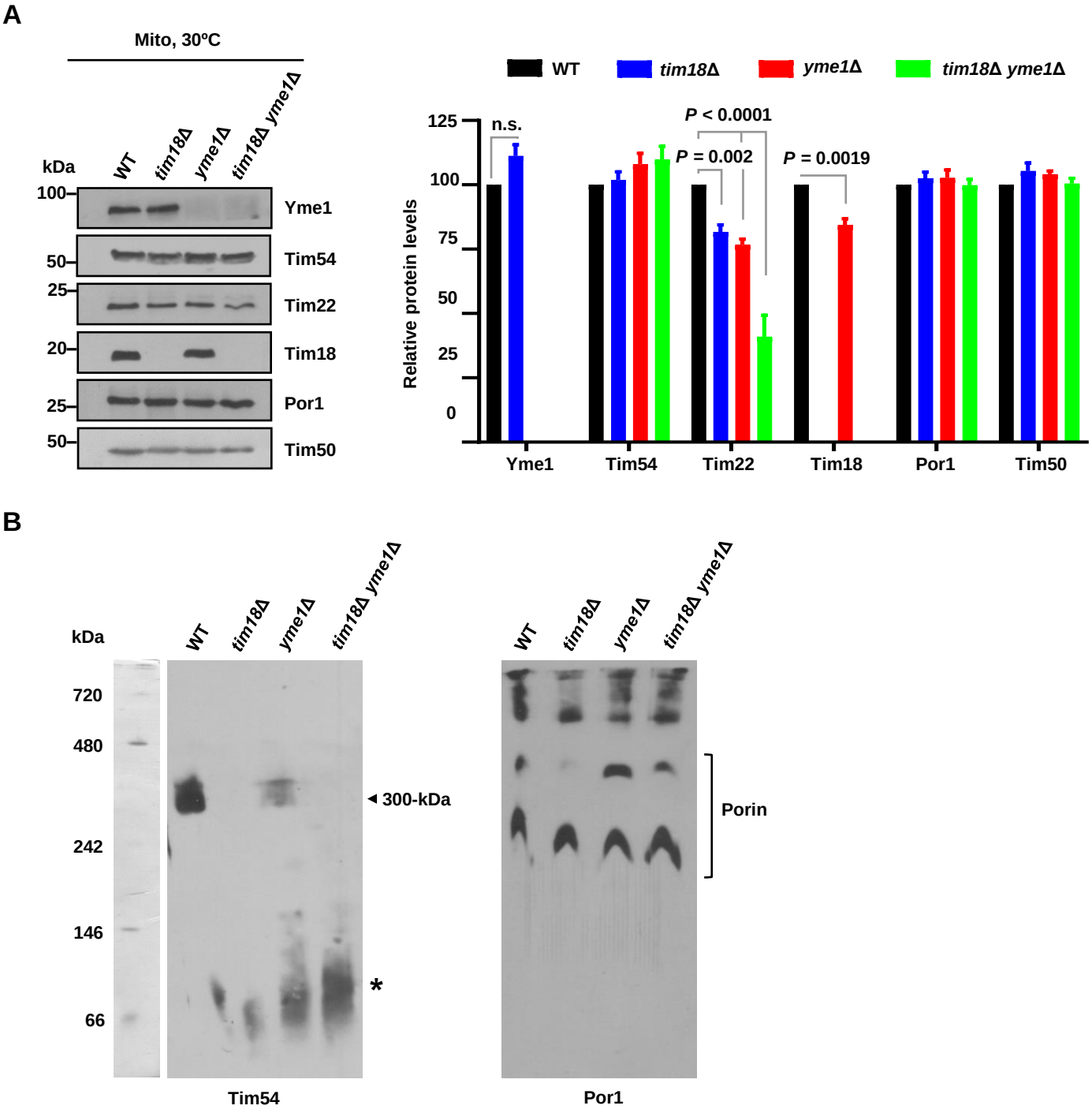

Fig. S5. The loss of Yme1 affects the steady-state levels of the TIM22 complex components. (A) Measurement of the protein levels of the carrier translocase machinery. 100 μg of mitochondria isolated from indicated strains grown in YPG medium at 30°C were assessed by immunoblotting. Protein amounts were quantified using ImageJ software and were plotted as percentages by setting the intensities of WT mitochondria as 100%. Data specify mean±s.e.m. of *n*=3 biological replicates. Two-way ANOVA with Tukey's multiple-comparisons test was used for calculating statistical significance. n.s., not significant. (B) Analysis of the stability of the carrier translocase machinery using BN-PAGE. Mitochondria isolated from WT, *tim18*Δ, *yme1*Δ, *and tim18*Δ *yme1*Δ cells grown at 37°C in YPG for 24 h were solubilized in digitonin buffer, and proteins were examined by BN-PAGE followed by immunoblotting with the indicated antibodies. Arrowhead represents the TIM22 complex (~300-kDa), and the asterisk indicates possible intermediate subcomplexes. The data shown are representative of *n*=3 biological replicates.

Fig. S6. Blot transparency

Fig. 1

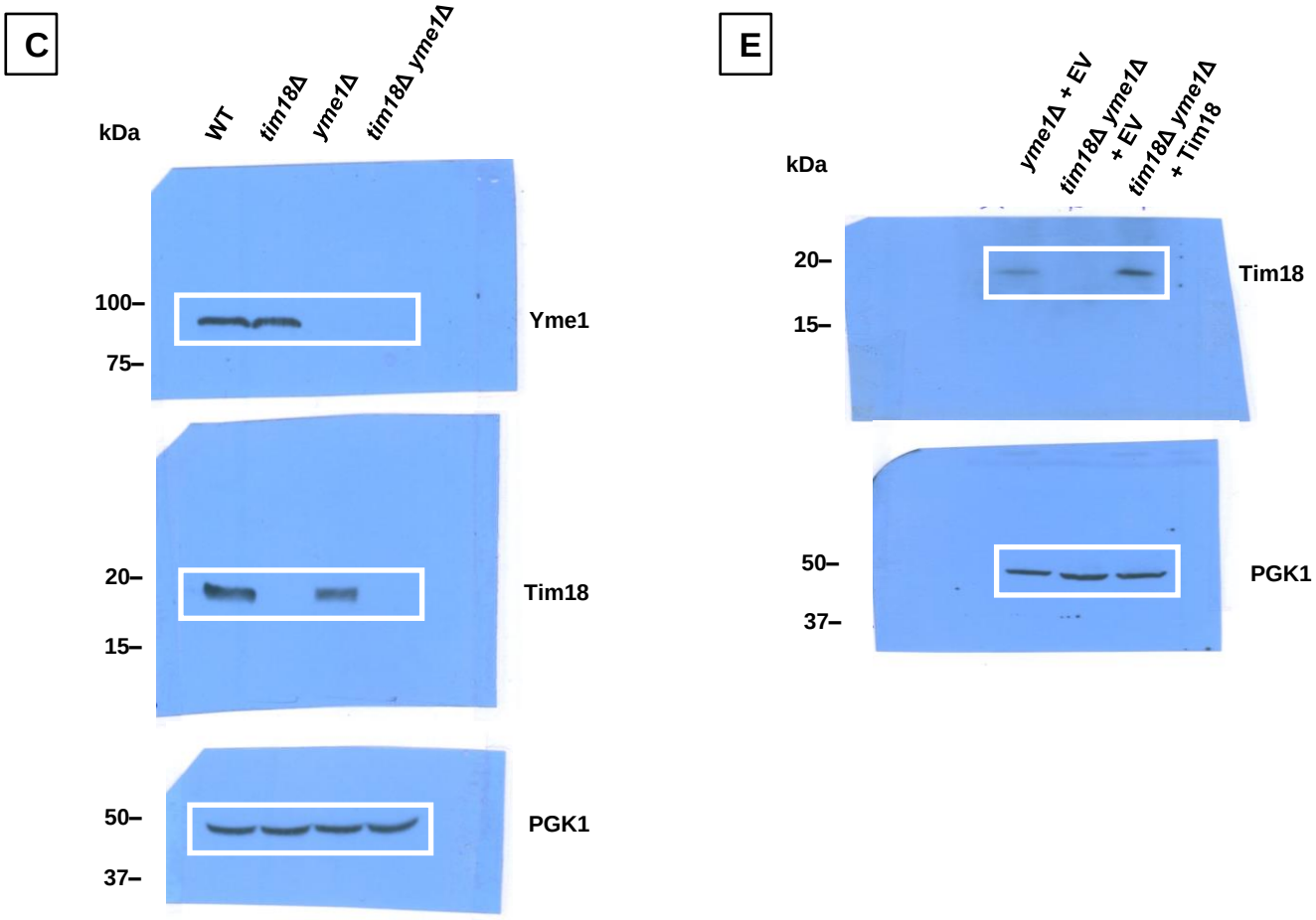

Fig. 3

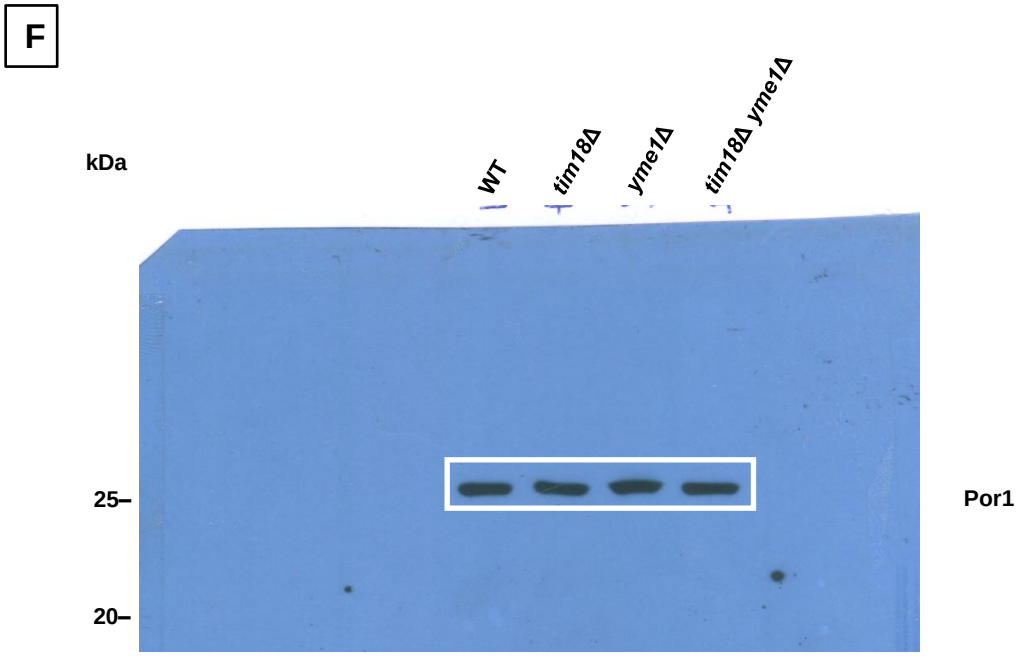

Fig. 4

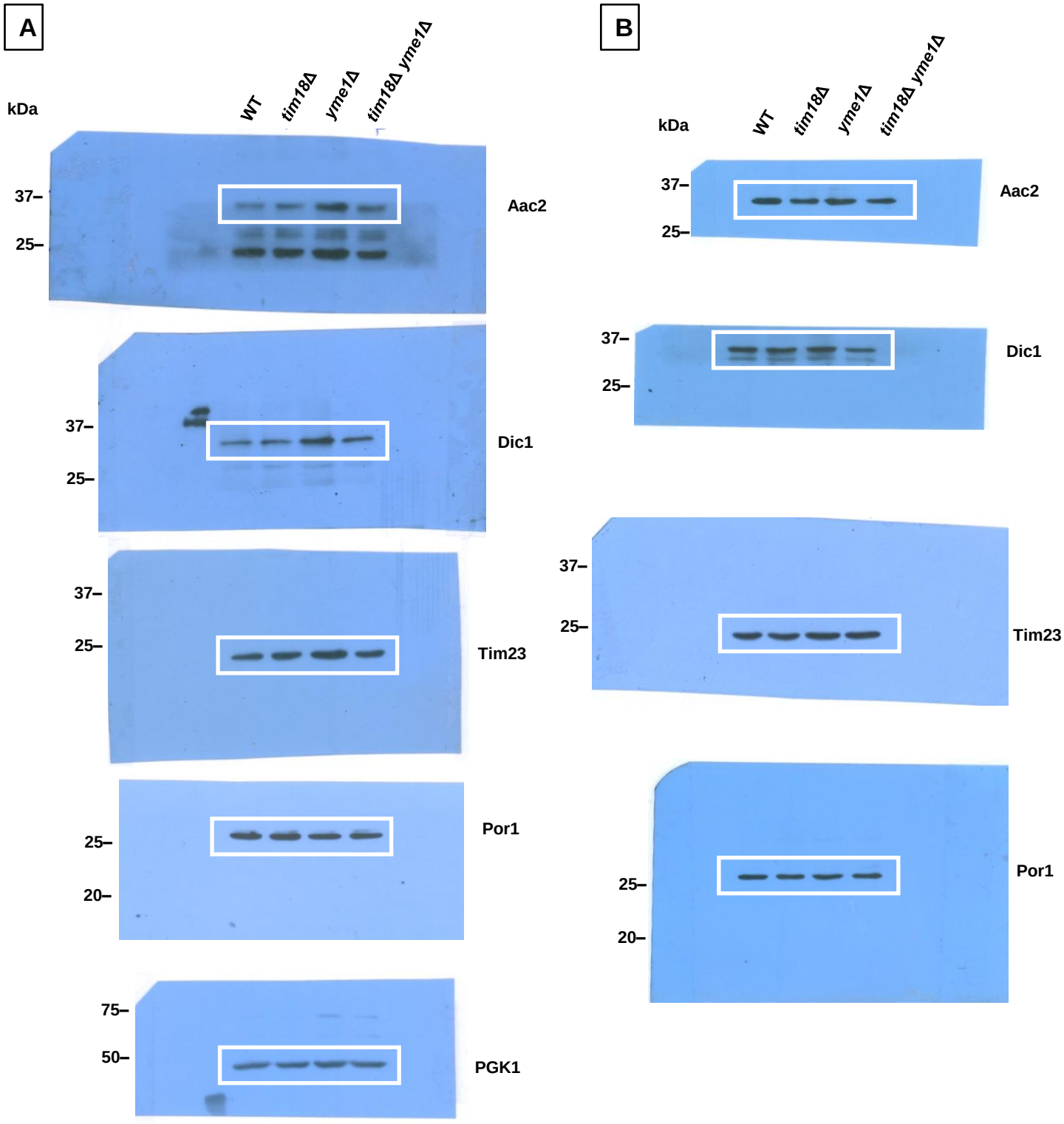

Fig. 5

B

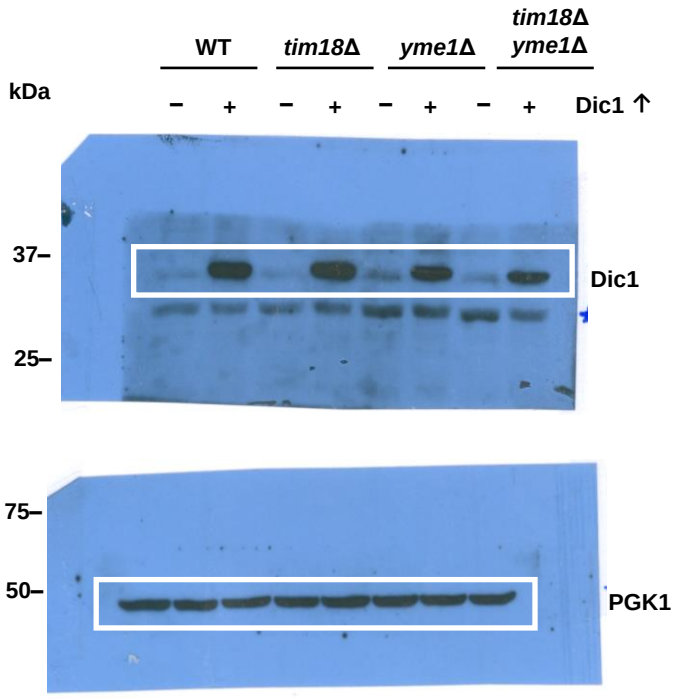

Fig. 6

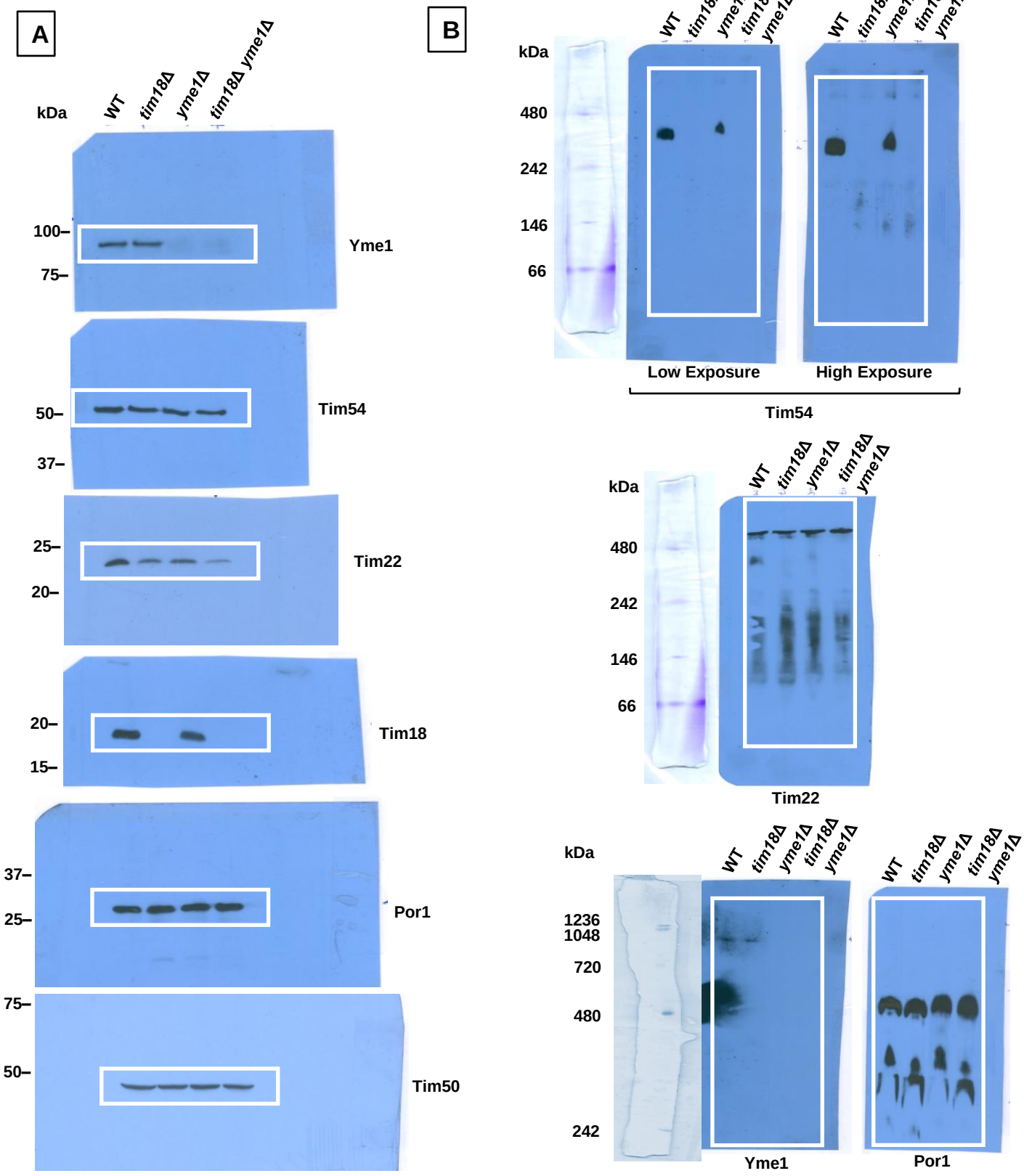

Fig. 6

C

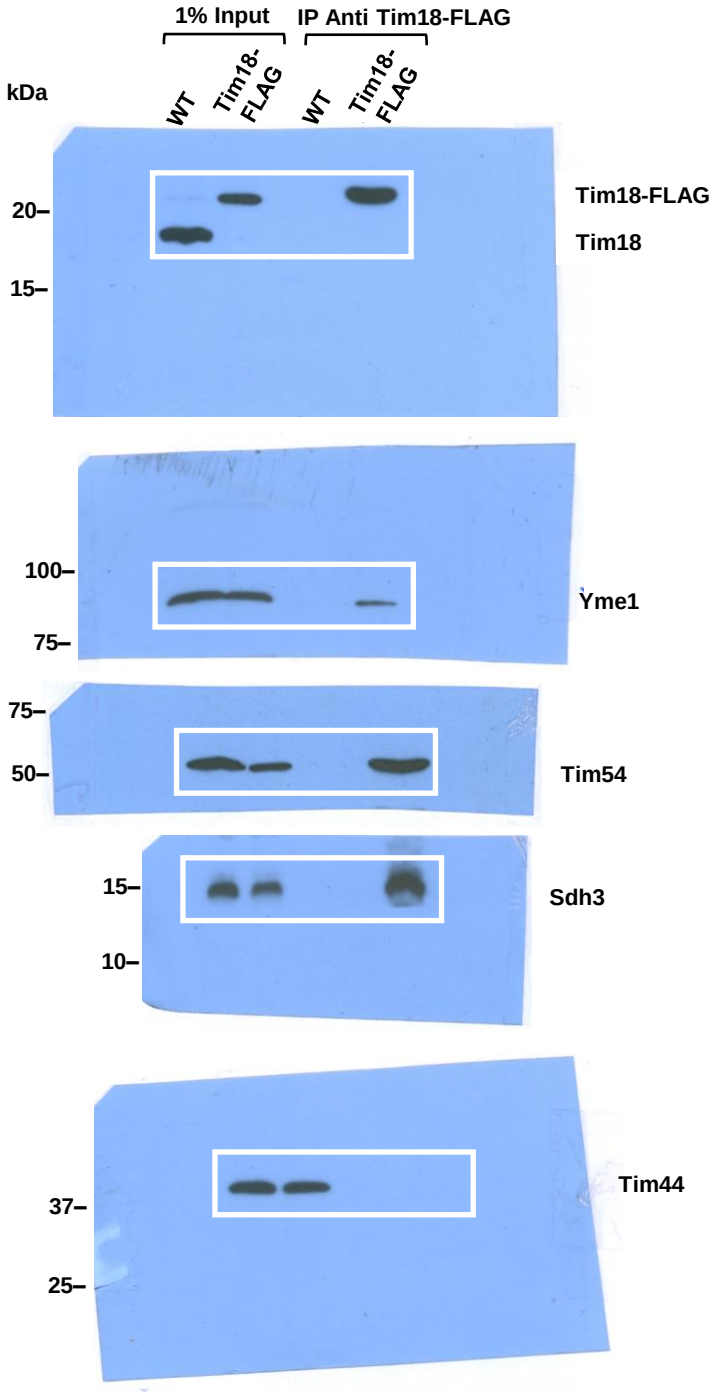

Fig. 6

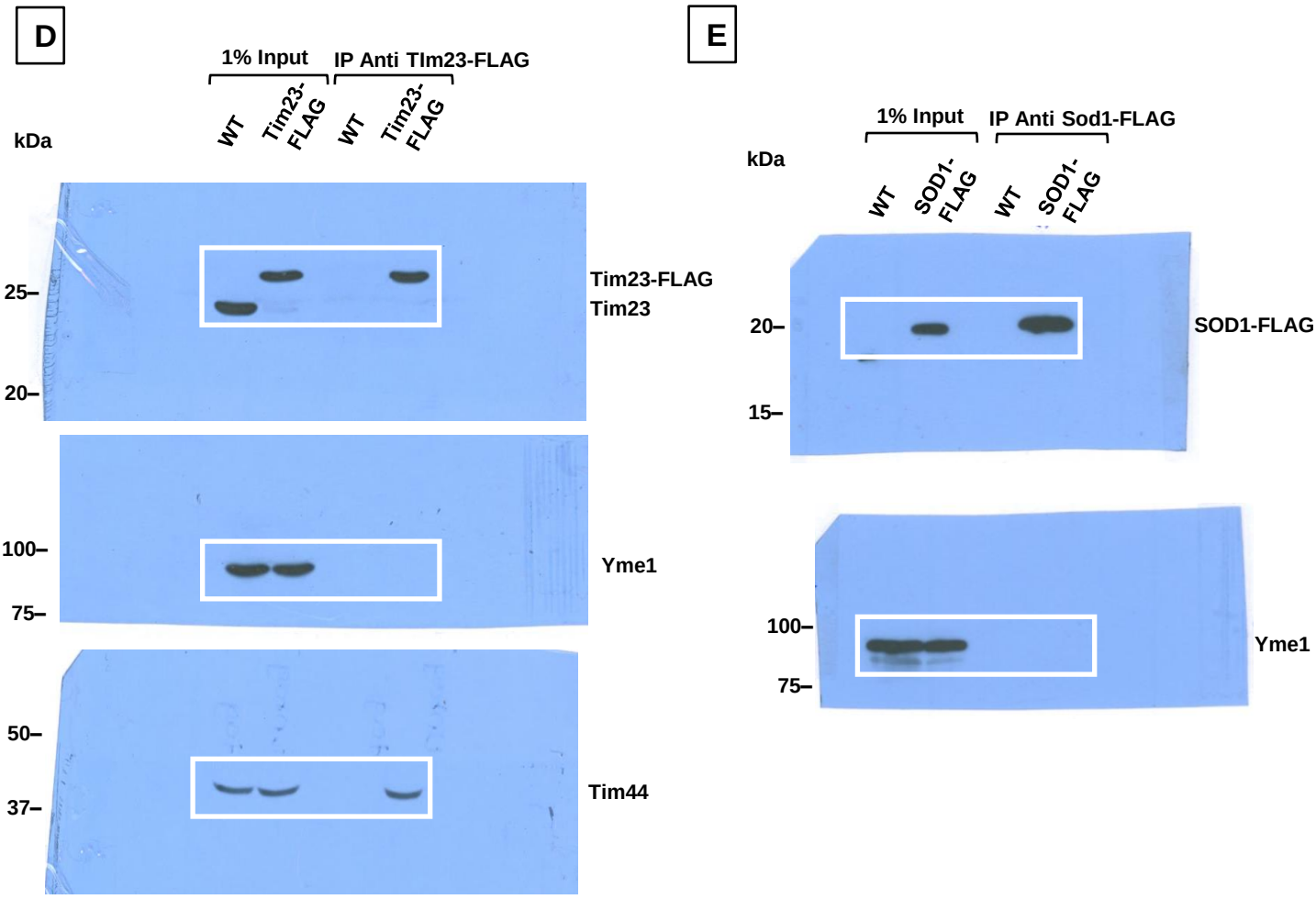

Fig. S1

C

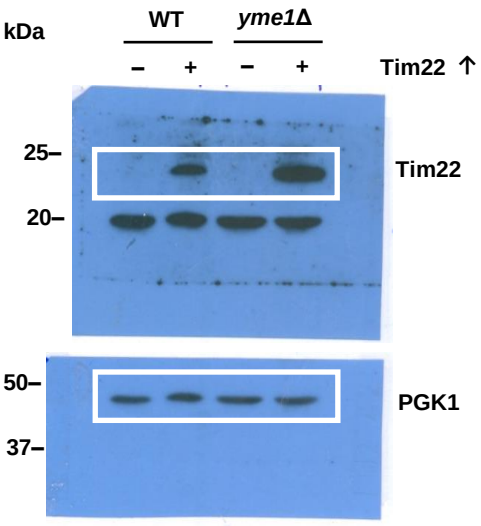

D

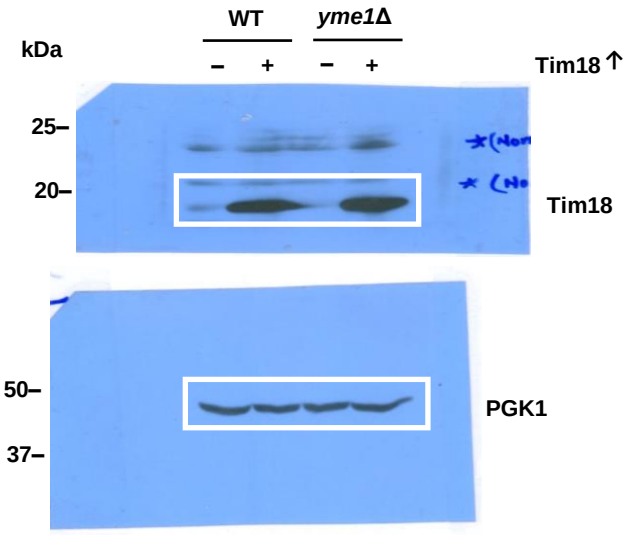

Fig. S3

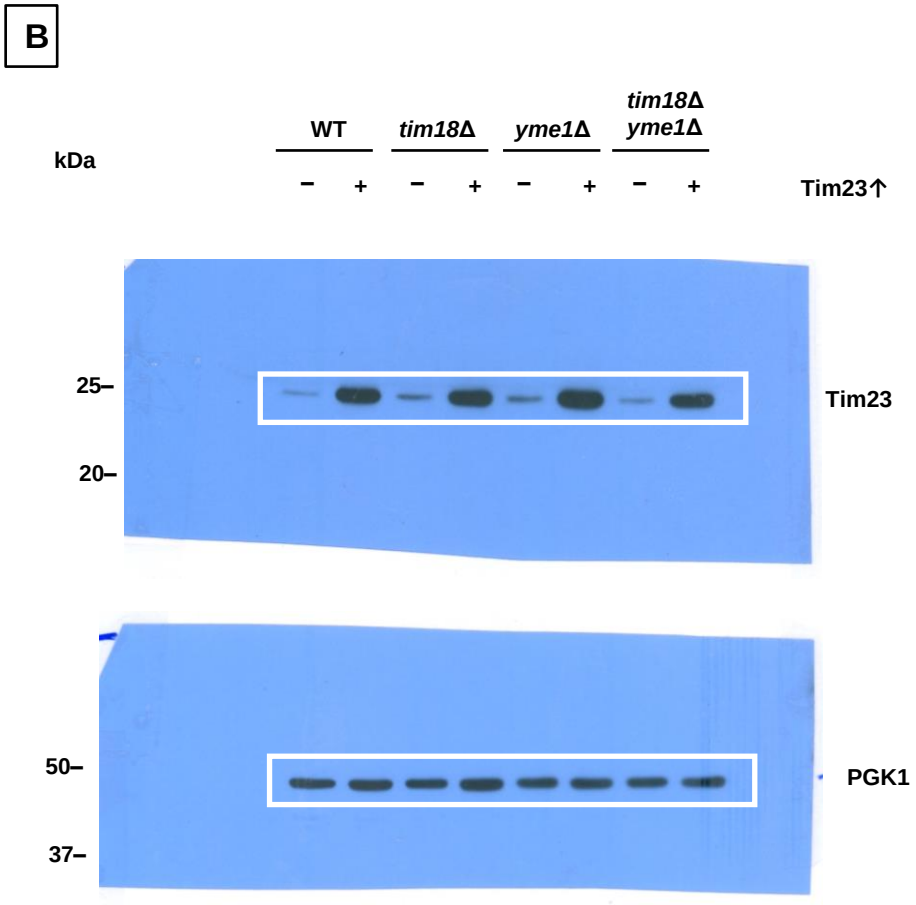

Fig. S4

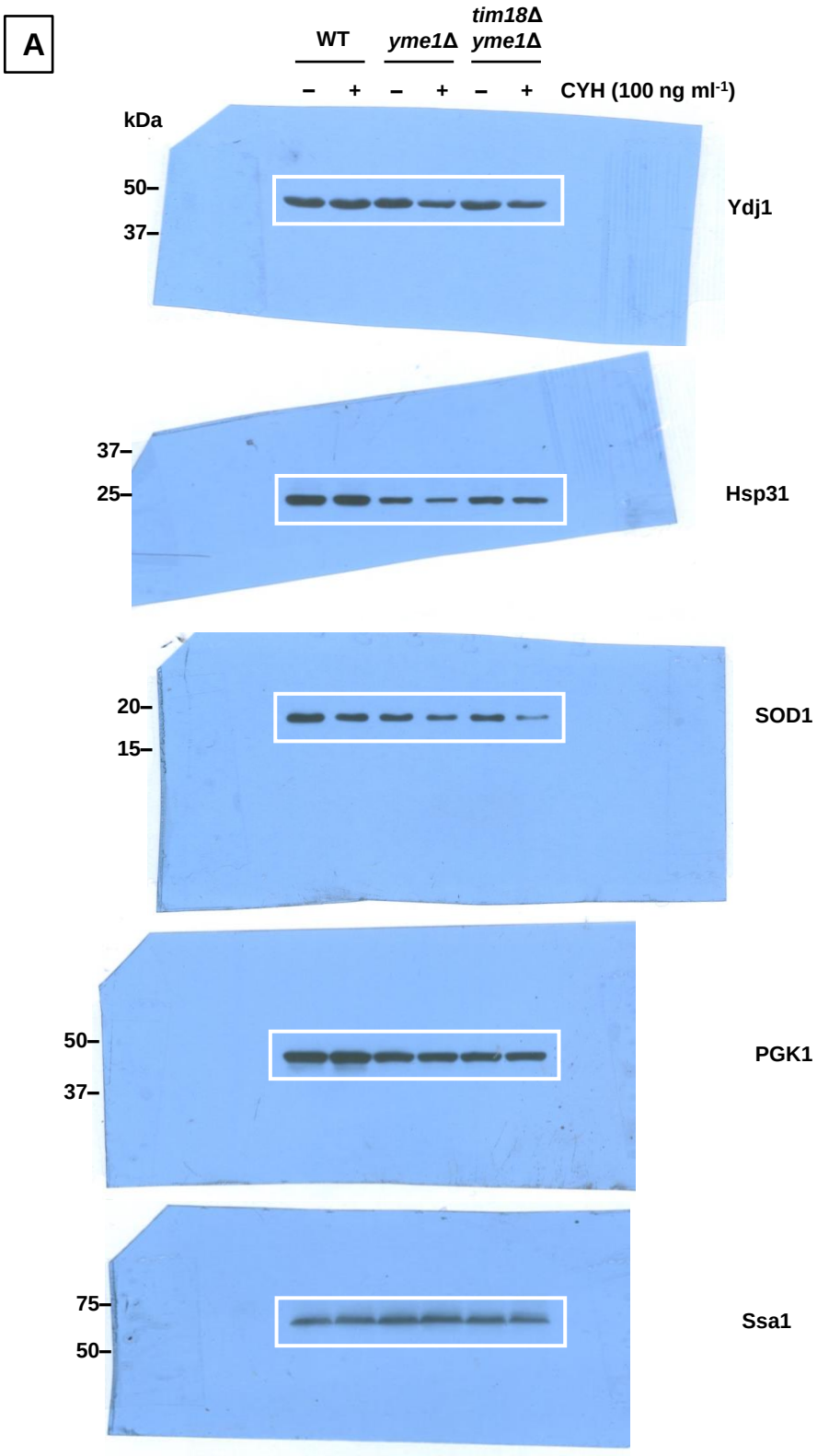

Fig. S4

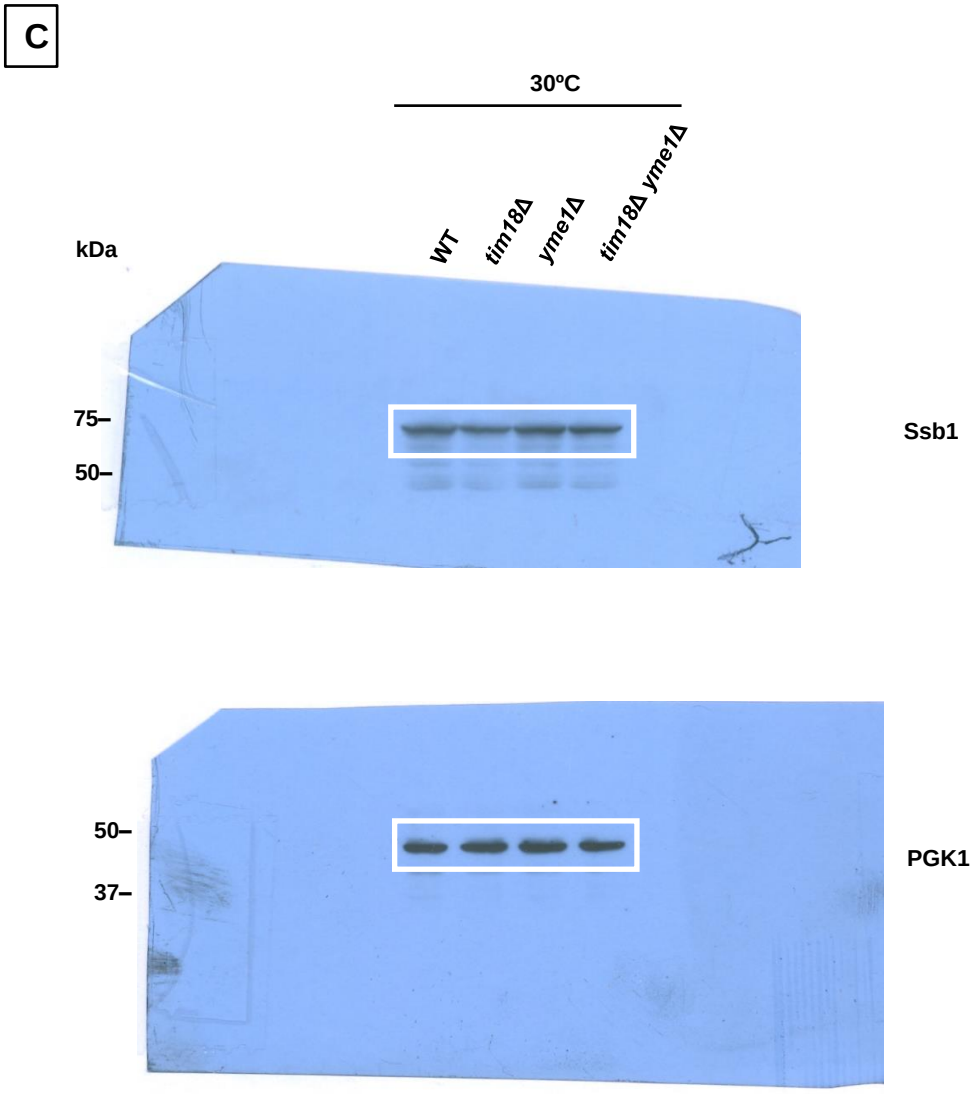

Fig. S4

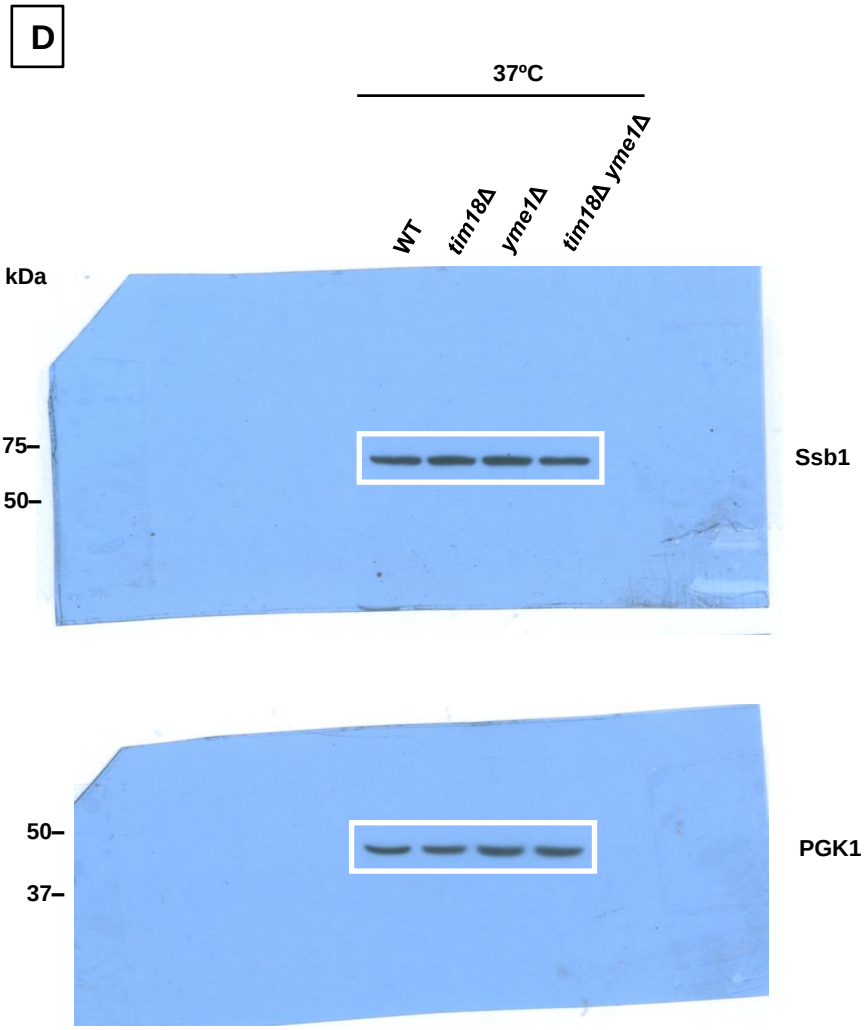

Fig. S5

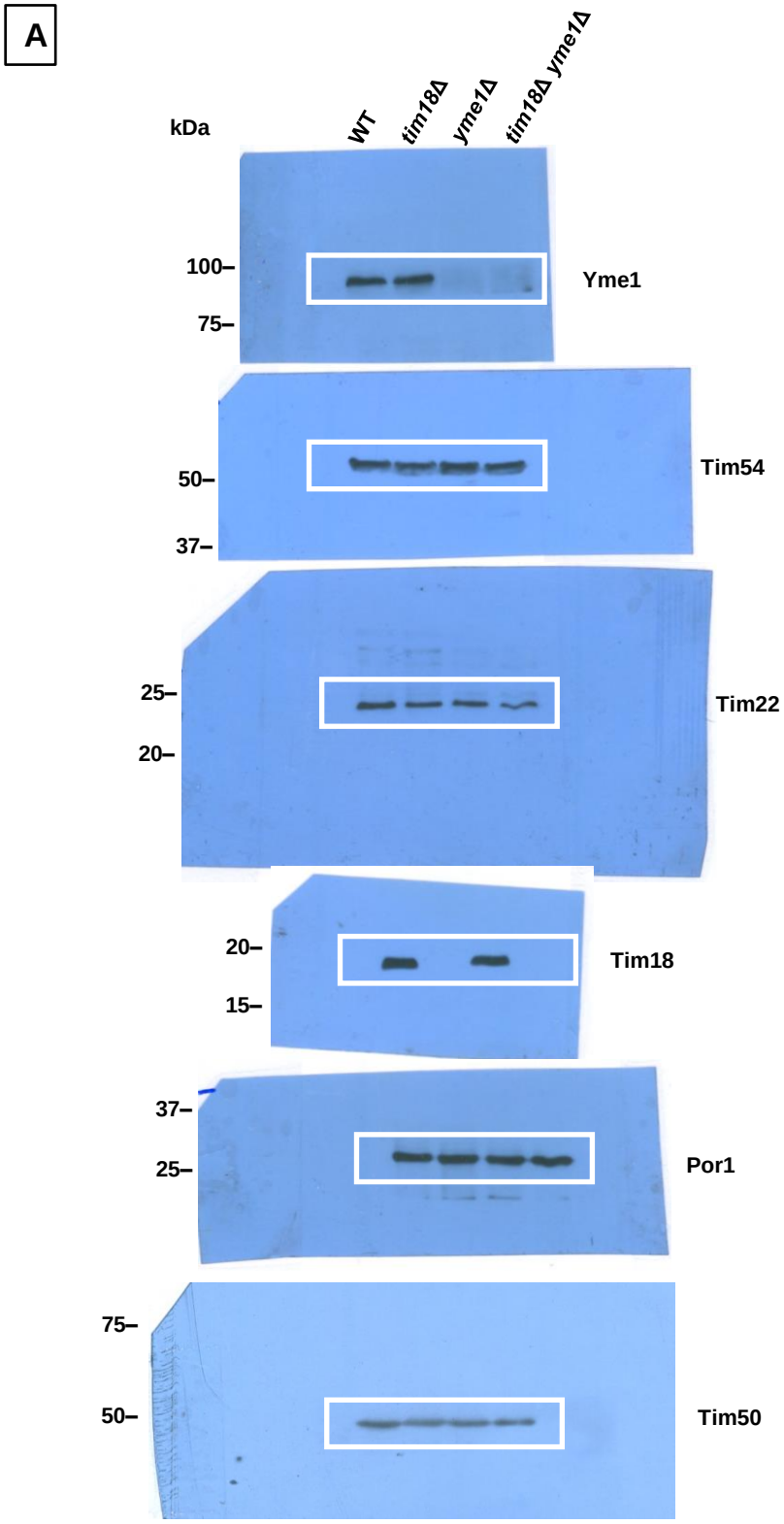

Fig. S5

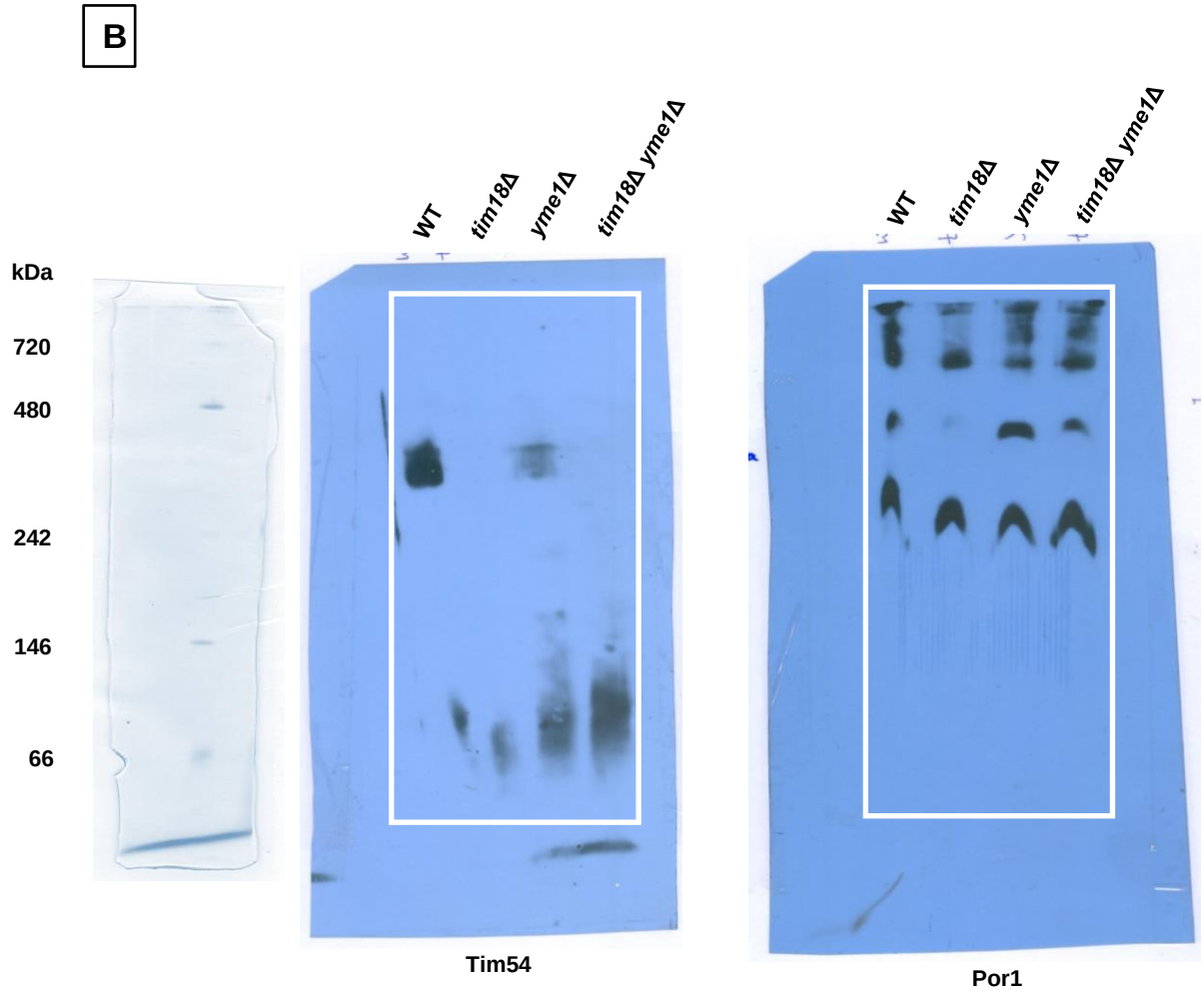

Table S1. Yeast strains used in this study

Name	Genotype	Source
WT W303	*MATa ade2-1 his3-11, 15 ura3-1 leu2-3, 112 trp1-1 can1-100 GAL2 met2-1 lys2-2*	Hines et al., 2011
tim18Δ	*MATa ade2-1 his3-11, 15 ura3-1 leu2-3, 112 trp1-1 can1-100 GAL2 met2-1 lys2-2 tim18Δ::KanMX4*	This study
yme1Δ	*MATa ade2-1 his3-11, 15 ura3-1 leu2-3, 112 trp1-1 can1-100 GAL2 met2-1 lys2-2 yme1Δ::HphNT1*	This study
tim18Δ yme1Δ	*MATa ade2-1 his3-11, 15 ura3-1 leu2-3, 112 trp1-1 can1-100 GAL2 met2-1 lys2-2 tim18Δ::KanMX4 yme1Δ::HphNT1*	This study
K127A *yme1Δ*	*MATa ade2-1 his3-11, 15 ura3-1 leu2-3, 112 trp1-1 can1-100 tim22Δ::CgHIS3* [pRS314-$tim22_{K127A}$] *yme1Δ::HphNT1*	This study
WT Tim22-316	*MATa ade2-1 his3-11, 15 ura3-1 leu2-3, 112 trp1-1 can1-100 tim22 Δ::CgHIS3,* [pRS316-*Tim22*]	Okamoto et al., 2014
Tim18FLAG/WT Tim22-316	*MATa ade2-1 his3-11, 15 ura3-1 leu2-3, 112 trp1-1 can1-100 tim22 Δ::CgHIS3, TIM18-FLAG::KanMX6* [pRS316-*Tim22*]	Okamoto et al., 2014
PTY44	*MATa lys2 ura3-52 leu2-3,112 trp1-Δ1 [rho$^+$ TRP1]*	Thorsness et al., 1993
PTY44/*tim18Δ*	*MATa lys2 ura3-52 leu2-3,112 trp1-Δ1 tim18Δ::KanMX4 [rho$^+$ TRP1]*	This study
PTY52	*MATa lys2 ura3-52 leu2-3,112 trp1-Δ1 yme1-Δ1::URA3 [rho$^+$ TRP1]*	Thorsness et al., 1993
PTY52/*tim18Δ*	*MATa lys2 ura3-52 leu2-3,112 trp1-Δ1 yme1-Δ1::URA3 tim18Δ::KanMX4 [rho$^+$ TRP1]*	This study
PJ53/Tim23-FLAG	*trp1-1/trp1-1, ura3-1/ura3-1, leu2-3,112/leu2-3/112, his3-11,15/his3-11,15 ade2-1/ade2-1, can1-100/can1-100 GAL2$^+$/GAL2$^+$, met2-Δ1/met2-Δ1, lys2-Δ2/lys2-Δ2, TIM23-FLAG::KanMX4*	This study
PJ53/SOD1-FLAG	*trp1-1/trp1-1, ura3-1/ura3-1, leu2-3,112/leu2-3/112, his3-11,15/his3-11,15 ade2-1/ade2-1, can1-100/can1-100 GAL2$^+$/GAL2$^+$, met2-Δ1/met2-Δ1, lys2-Δ2/lys2-Δ2, sod1Δ::HphNT1* [pRS416$_{GPD}$-*SOD1-FLAG*]	This study

Table S2. Plasmid constructs and primers used in this study

	Primers used for deletion of *TIM18* and *YME1*gene	
Construct Name	**Orientation (5'-3')**	**Source**
*tim18*Δ Fwd	CGGTGATGCGAGGTGCAACAACTGAGTAATTTAATACCTTTGGCGTACGCTGCAGGTCGAC	This study
*tim18*Δ Rev	GAAATCTTAGAAATGCAAAAAAAAAGAAAAAGTATGGGTGAGTCAATCGATGAATTCGAGCTCG	This study
*yme1*Δ Fwd	GCAATTTTTAATTATAATACATTGTGGATAGAACGAAAACAGAGACGTGCGTACGCTGCAGGTCGAC	This study
*yme1*Δ Fwd	CGGTCTTGAGGTAGGTTCCTTCATACGTTTAACTTCTTAGAATAAAATCAGGATGGCGGCGTTAGTATCG	This study

	Primers used for plasmid construction		
Construct Name	**Orientation (5'-3')**	**Restriction Site**	**Source**
pRS316-Tim18 Fwd	GCGAGCGGCCGCAAAGTTTAGGTCATCACTTCCC	NotI	This study
pRS316-Tim18 Rev	ACGCGTCGACATAATAAAAAAGGCACTTTAGA	SalI	This study
$pRS416_{TEF}$-Tim22 Fwd	GCGGGATCCATGGACTACAAAGACGATGAC	BamHI	This study
$pRS416_{TEF}$-Tim22 Rev	ACGCGTCGACTCATTCTTTAAAATCGTTTTG	SalI	This study
$pRS416_{TEF}$-Tim18 Fwd	GCGTCTAGAATGCTATTGTTTCCTGGCTTGAAG	XbaI	This study
$pRS416_{TEF}$-Tim18 Rev	ACGCGTCGACTTAACGGGTGTTTTGCAACC	SalI	This study
$pRS414_{TEF}$-AAC2 Fwd	CGCGGATCCATGTCTTCCAACGCCCAAG	BamHI	This study
$pRS414_{TEF}$-AAC2 Rev	ACGCGTCGACTTATTTGAACTTCTTACC	SalI	This study

pRS414$_{TEF}$-PIC Fwd	CTAGACTAGTATGTCTGTGTCTGCTGCTCC	SpeI	This study
pRS414$_{TEF}$-PIC Rev	CCGCTCGAGCTAATGACCACCACCACC	XhoI	This study
pRS414$_{TEF}$-DIC1 Fwd	CGCGGATCCATGTCAACCAACGCAAAAGAG	BamHI	This study
pRS414$_{TEF}$-DIC1 Rev	ACGCGTCGACCTACTTGTCTTCCTTTGGC	SalI	This study
pRS414$_{TEF}$-Tim23 Fwd	CGGACTAGTATGTCGTGGCTTTTTGGAG	SpeI	This study
pRS414$_{TEF}$-Tim23 Rev	CCGCTCGAGTCATTTTTCAAGTAGTCTTTTC	XhoI	This study
pRS414$_{TEF}$-Tom6 Fwd	CGCGGATCCATGGACGGTATGTTTG	BamHI	This study
pRS414$_{TEF}$-Tom6 Rev	ACGCGTCGACTTATAATTGTGGGGCC	SalI	This study
pRS414$_{TEF}$-Abf2 Fwd	CGCGGATCCATGAACAGTTACAGCCTATTA	BamHI	This study
pRS414$_{TEF}$-Abf2 Rev	CCGCTCGAGCTAGTTGAGAGGGTAGCGAGC	XhoI	This study
pRS416$_{GPD}$ SOD1 Fwd	CGCGGATCCATGGTTCAAGCAGTCGCAGTG	BamHI	This study
pRS416$_{GPD}$ SOD1 Rev	TGCGGTCGACTTACTTGTCGTCATCGTCTTTGTAG TCGTTGGTTAGACCAATGACACC	SalI	This study

*** Restriction sites are underlined**